MAT JOURNALS

Journal of Industrial Mechanics
Volume 3 Issue 3

A Review of Blowing: as an Active Flow Control Strategy

Kh. Md. Faisal
Assistant Professor
Department of Aeronautical Engineering, Military Institute of Science and Technology
Mirpur Cantonment, Dhaka, Bangladesh.
Email: *faisal.ae.mist@gmail.com*

Abstract

Flow control has significant technological importance as it can manipulate the flow field in a desired way either actively or passively. This wide research area has remained the point of attention for many years as it is applicable to various applications. Blowing as a flow control method, among other methods, is more technically feasible and market ready technique. A brief review from the existing literature on various studies on blowing has been presented along with their outcome. Then, studies were conducted to investigate the performance variation (in terms of lift coefficient, drag coefficient) of different airfoils with respect to various blowing parameters. It was observed that for NACA 0012 airfoil the maximum lift coefficient peaks at a blowing ratio 0.2 and then it decreases whereas the stalling angle increases with rise of blowing ratio. For LA203A both maximum lift coefficient and stalling angle increases with blowing ratio. For thick airfoil, it was found that lift increases with the rise of moment coefficient and blowing ratio and mid chord slots gives better performance at lower angles of attack whereas leading edge slots exhibits better performance at higher angles of attack. In case of thick elliptical airfoil, increase in lift coefficient was noticed with the increase in moment coefficient and blowing ratio but an optimum jet width to chord ratio (0.41) was found beyond which increase in jet width causes drop in lift coefficient. Additionally, it was found that at lower blowing angle thick elliptical airfoil performs better compared to that of higher angles of attack. Study on NACA 0012 and Aerospatiale A proved the fact that lifts increases with rise in blowing ratio at three different jet diameters to chord ratios. This study also found that higher blowing ratio is also advantageous for the turbo machinery in increasing the pressure difference. Lastly, the study on low Re airfoil flow found that increasing blowing ratio has a deleterious effect on aerodynamics performance (in terms of lift and drag coefficient).

Keyword: *Airfoil, NACA, Aerospatiale, LA203A*

INTRODUCTION

Flow control attempts to alter a natural flow state or development path into a more desired state. This can be accomplished in two ways (active or passive). Active flow control requires external energy (electrical or mechanical), whereas passive flow control does not require external energy. The major drawback with the passive flow control is that it will increase the profile losses and it cannot be deactivated when it is not required. Thus, active flow control becomes important.

Active flow control is applied in various fields of application. Some of them are fixed wing airfoil applications, turbo machinery applications, combustion control, aero acoustics, air-breathing propulsion, rotorcraft applications etc.

From the very beginning, human being has been always dissatisfied with the existing world that surrounds him and tried to achieve superiority through controlling it to get more beneficial effects. This applies to almost all disciplines of science and technology. Thus, gaining control over the

Page 1-33 © MAT Journals 2018. All Rights Reserved

behavior of mechanical systems is an essential concept that inescapably arises in research fields starting from dynamics and robotics [1-3] to fluid mechanics [4-6] and boundary layers. This concept gives the birth of the discipline of Flow Control. Under the general heading of flow control, techniques are developed to manipulate the boundary layer, either to increase the lift or decrease the drag [7]. Flow control techniques give the ability to attain significant variations in flow behaviour with little amount of energy input. This infers that some magnifying mechanism exists in the flow for which the actuator triggers, enhances or suppresses in some way [8]. Like many other fields, the benefits of flow control have become more important in the field of aviation. As the price of fuel is increasing, to reduce the need for fuel, drag is to be reduced. This demand has led to the demand for increased lift-to-drag ratio. This ratio becomes critical during take-off and landing, as the wings of airplanes require generating an enormous amount of lift at low flight velocity. In modern commercial aircraft, complex multi-element high-lift devices realize this. As these causes added weight, increased constructive effort, etc., there is an important economic interest in substituting the multi-element devices by single flaps. But flaps are only applicable if flow separation at high flap angles can be controlled. Here, arises the necessity of flow control. According to Flatt, flow control or boundary layer control comprises any mechanism or process for which the boundary layer of a fluid flow is caused to behave differently than it normally would when the flow develops naturally along a surface. Methods to achieve transition delay, separation delay, lift augmentation, drag decrease, turbulence augmentation, and noise suppression have been considered as flow control methods [9]. The control of boundary layer transition and the elimination or delaying of the boundary layer separation have been studied by many researchers. For example, separation and transition phenomenon around a symmetric (NACA0012) airfoil at an angle of attack 4° and Reynolds number 10^5 have been studied by Shan [10]. Among the two ways of boundary layer control (active or passive), both are important in different situation. When changing flow conditions are not the serious issue, passive technologies offer simple solution. But, active flow control becomes vital when it is necessary to react to rapidly changing flow conditions [11]. In active boundary layer control, momentum injection into the boundary layer region causes delay in flow separation as it increases the energy of the boundary layer and keeps it attached to the profile [12].

Pulsed blowing is also a way of active boundary layer control, the effect of which on control performance was studied by Hecklau [13] and Deng [14]. In most cases excitation is incorporated at the leading edge to affect the boundary layer upstream of the point of separation, with suction and blowing (steady or periodic) [15]. Prevention of separation gives rise in lift and reduction in drag. Suction and blowing of primary fluid can have significant effects on the flow field, manipulating mainly the shape of the velocity profile close to the wall and thus the boundary layer vulnerability to transition and separation [16].

Many literatures are available on research histories on flow control techniques [17-19]. A two-volume monograph edited by Lachmann up to 1960 (1961) [20] and more recent by Mohammad Gad-el-Hak up to 2000[21] give a great review of researches on flow control techniques. These methods, have been investigated in different ways like analytically [22-24], experimentally [25-33] and numerically [34-35]. The first scientist who employed boundary layer suction to delay boundary

Page 1-33 © MAT Journals 2018. All Rights Reserved

layer separation in 1904 was Prandtl [36]. In the late 1930s and the1940s experiments were conducted on boundary layer suction for wings [37-39]. A lot of numerical works were carried out on well-known NACA airfoils regarding the measurement of lift and drag coefficients under different flow conditions [40-44]. Flow control techniques (such as suction and blowing) on a NACA 0012 airfoil were studied by Huang [45]. His study revealed that when jet location and angle of attack were combined, perpendicular suction at the leading edge increased lift coefficient better than other suction situations. For tangential blowing, downstream locations were found to lead to the maximum increase in the lift coefficient value. The effect of changing location of secondary blowing on the performance of control was investigated by Zheng [46]. It was found that when the secondary blowing slot was located close to the separation point, better control was obtained because the boundary layer thickness is less at the commencement of separation. A very significant parameter in separation control is blowing ratio (i.e., the ratio of secondary blowing velocity to free stream velocity) as it determines how much momentum is to be supplied to the flow. The effect of this parameter was studied by Ludeweig [47]. Flow separation control through fluid injection was numerically investigated by Rosas [48] and it was found that lift coefficient increased dramatically. An evolutionary algorithm to optimize flow control was given by Beliganur and Raymond [49]. They showed that the use of two suction jets along with two blowing jets enhanced the lift-to-drag ratio for a NACA 0012 airfoil. Control effects on NACA 0012 airfoil with a spanwise blowing located at 0, 25 and 100% from the leading edge at the angle of attack from -20° to 20° was investigated by Wong [50]. Flow separation delayed by periodic vertical suction and blowing through a slot close to the leading edge of the flap was studied by Schatz and Thiele [51]. The effects of steady blowing flow separation control technique were analyzed by Svorcan et al. [52]. Three different flow fields were considered including subsonic flow past an Aerospatiale A airfoil, transonic flow past a NACA 0012 airfoil, and transonic flow in linear compressor/turbine cascade. It was found that lift coefficients and lift-to-drag ratios are improved for all controlled cases. The influences of a passive flow control method on the aerodynamic performance of S809 airfoil was investigated by Moshfeghi[53]. For this, the airfoil was splitted along the span and the effects of split location on low-speed shaft torque, power coefficient and flow patterns were investigated numerically. It was found that the torque is quite sensitive to the split location. One way of passive flow control is using vortex generators. These may be of different shapes like split-ramp, ramp and ramped vane etc. which were studied by Lee [54]. He showed that these can be effective even in case of supersonic speed. Using surface roughness is another way of passive flow control. Surface roughness can have significant effect on the aerodynamic performance of turbo machinery (like turbine) which was investigated by Bie [55]. One researcher Bruneau [56] showed that the simultaneous application of active control techniques with passive techniques is very effective for controlling boundary layer separation.

With the development of computational facilities in recent years, computational fluid dynamics (CFD) has been increasingly used to investigate flow control. Numerous flow control studies through CFD approaches [57-65] have been conducted to investigate the effects of blowing, suction, and synthetic jets on the aerodynamic characteristics of airfoils. So, a good number of researches have been conducted in a various way covering

Page 1-33 © MAT Journals 2018. All Rights Reserved

a numerous aspects of flow control.

This report is going to present different studies those were conducted on various airfoils to investigate their variation in aerodynamic performance under the influence of various blowing parameters. Under the heading of problem formulation and experimental/numerical setup, governing equations as well as discussion related to experimental/numerical setup that were used in those studies are presented. Then, under the heading of results and discussions, the outcome of the different studies is presented along with the discussion of underlying physics. A combined conclusion of all those studies are given under the conclusion which is followed by future direction of research.

Problem Formulation and Experimental/Numerical Setup

Study of blowing on NACA 0012 and LA203A airfoils

This section presents the governing equations that were used as well as relevant discussion on simulation setup for investigating the effect of blowing on the performance of NACA 0012 and LA203A airfoils.

The following governing equations were used for this study:

In this study the flow is steady, incompressible and two-dimensional. Governing equations used in this study are given in general form:

Continuity equation: $\frac{\partial u_i}{\partial x_i} = 0$ (1)

Momentum equation: $\frac{\partial u_j}{\partial t} + u_i \frac{\partial u_j}{\partial x_i} = -\frac{1}{\rho}\frac{\partial p}{\partial x_i} + \vartheta \Delta u_j$ (2)

Energy equation: $\frac{\partial E}{\partial t} + u_i \frac{\partial E}{\partial x_i} = \emptyset + \frac{1}{\rho}\frac{\partial}{\partial x_i}[k\frac{\partial T}{\partial x_i}]$ (3)

Equation of state: $P = \rho RT$ (4)

In these equations u represents component of velocity, j is the fixed index, i is the variable index, p is the static pressure, ϑ is the kinematic viscosity, ρ is the density, E is the internal energy per unit mass, Ø is the viscous dissipation function per unit mass, R is the characteristic gas constant and T is the temperature.

The following turbulence model was selected:

As standard turbulence model, the standard k-ε model is employed to conduct the analysis. Launder and Spalding proposed this model [66] which has a rational accurateness for a wide range of turbulent flows. Doing review on many literatures on this type of research it was found that for the current study this model will be a suitable one and hence it is selected. This model is constructed on model equations of turbulent kinetic energy and dissipation rate.

$$\frac{\partial(\rho k)}{\partial t} + \frac{\partial(\rho k u_i)}{\partial x_i} = \frac{\partial}{\partial x_j}\left[\left(\mu + \frac{\mu_t}{\sigma_k}\right)\frac{\partial k}{\partial x_j}\right] + G_k + G_b - \rho\varepsilon - Y_M + S_k \quad (5)$$

$$\frac{\partial(\rho \varepsilon)}{\partial t} + \frac{\partial(\rho \varepsilon u_i)}{\partial x} = \frac{\partial}{\partial x_j}\left[\left(\mu + \frac{\mu_t}{\sigma_k}\right)\frac{\partial \varepsilon}{\partial x_j}\right] + S_\varepsilon + C_{1\varepsilon}\frac{\varepsilon}{k}(G_k + C_{3\varepsilon}G_b) - C_{2\varepsilon}\rho\frac{\varepsilon^2}{k} \quad (6)$$

In above model equations, G_k characterises the generation of turbulence kinetic energy due to the mean velocity gradients, G_b stands for the generation of turbulence kinetic energy due to buoyancy, Y_M represents the contribution of the fluctuating dilatation in compressible turbulence to the overall dissipation rate, $C_{1\varepsilon}$, $C_{2\varepsilon}$ and $C_{3\varepsilon}$ are constants. σ_k and σ_ε are the turbulent Prandtl numbers for k and ε, respectively. S_k and S_ε are user-defined source terms.

The following geometries were taken into consideration:

NACA 0012 and LA203A are selected for this study. Airfoil coordinates for these airfoils are obtained from UIUC website. Geometry created from these coordinates were imported to ANSYS ICEM CFD. Chord length of the airfoils were taken 195 mm. The location of the slot for secondary injection was at 60 percent of the chord

Page 1-33 © MAT Journals 2018. All Rights Reserved

length from the leading edge and the length of the slot was taken as 1.4 percent of the chord length.

Fig: 1. *NACA 0012 [68]*

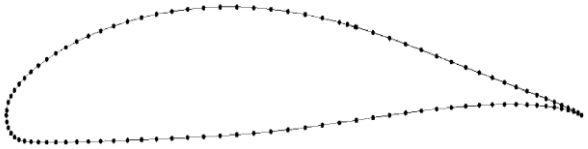

Fig: 2. *LA203A [68]*

Grid was generated in the following way

The computational domain was created in such a way so that there remains no boundary effect on the flow field surrounding the airfoil. An equal amount of distance (10 chord lengths) was maintained both from inlet and outlet of the domain to leading and trailing edge of the airfoils respectively. Likewise, the top and bottom far fields are also fixed at same distance away from the upper and lower sides of the airfoil. Computational domains for NACA 0012 and LA203A are presented in Figs. 3 and 4 respectively. ANSYS ICEM CFD was used to create grid. As boundary layer is created on airfoil surface so grid near the airfoil surface was denser to capture the boundary layer characteristics. Grid generated at leading edge and trailing edge of NACA0012 and LA203A airfoils are shown in Figs. 5 and 6. Grid surrounding the secondary inlet portion is displayed at Fig. 7. The type of grid generated was 2D planar grids and the number of quadrilateral cells were around 83,457.

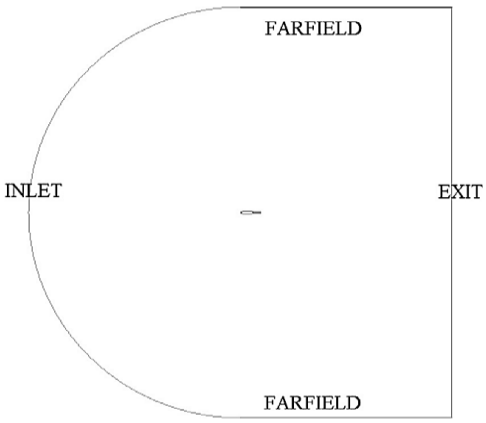

Fig: 3. *Computational domain of NACA 0012 [68]*

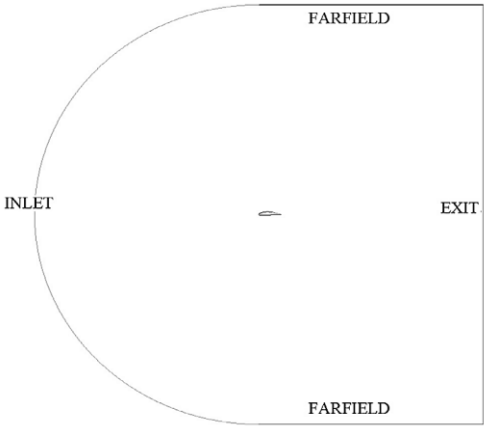

Fig: 4. *Computational domain of LA203A[68]*

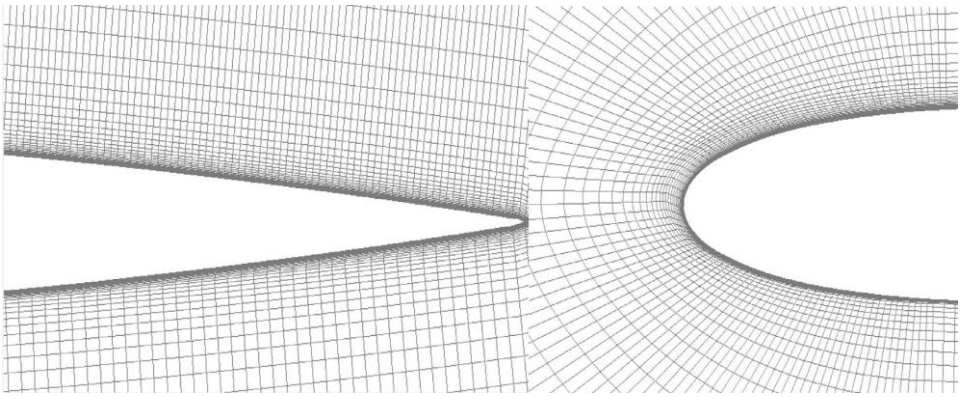

Fig: 5. *Close view of trailing edge and leading edge of NACA 0012 [68]*

Page 1-33 © MAT Journals 2018. All Rights Reserved

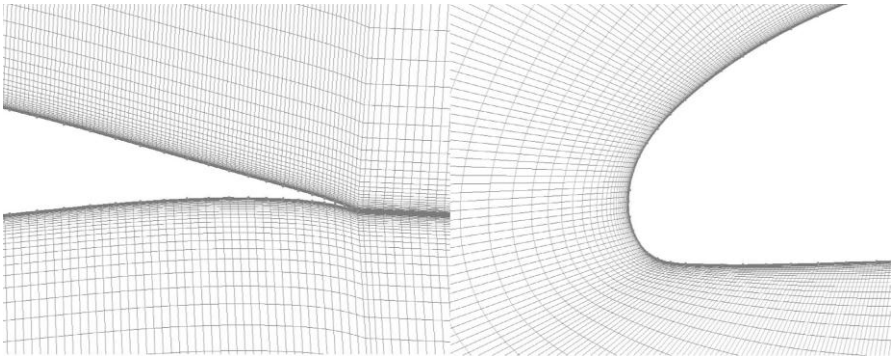

Fig: 6. *Close view of trailing edge and leading edge of LA203A [68]*

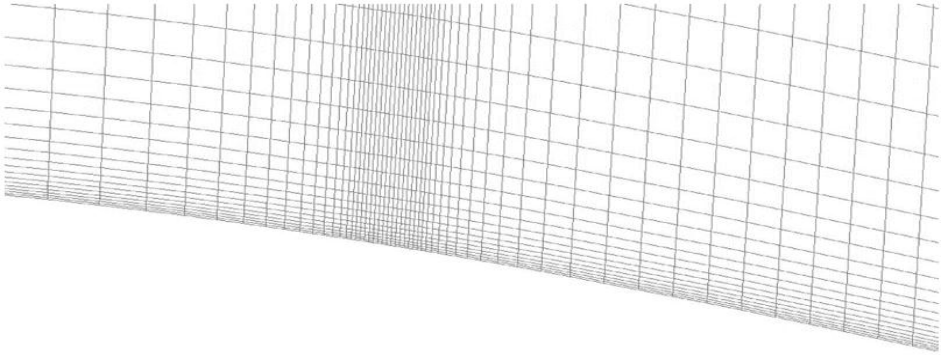

Fig: 7. *Close view of secondary inlet section [68]*

Study of Grid Independence

A grid independence study was conducted with four different grid densities on NACA0012 airfoil at 0 ° angle of attack and then the final grid was selected. The results of grid independence study are charted in Table 1 and Fig. 8. As it is evident from Fig. 8, that the value of C_L does not change that much with the change in cell number (from 83457 to 145867). So to reduce the computational time yet maintaining a reasonable accuracy, 83457 was selected as number of cell.

Table: 1. *Study of Grid Independence [68]*

No of cells	C_L
47978	0.2019
68987	0.1963
83457	0.1922
145867	0.1913

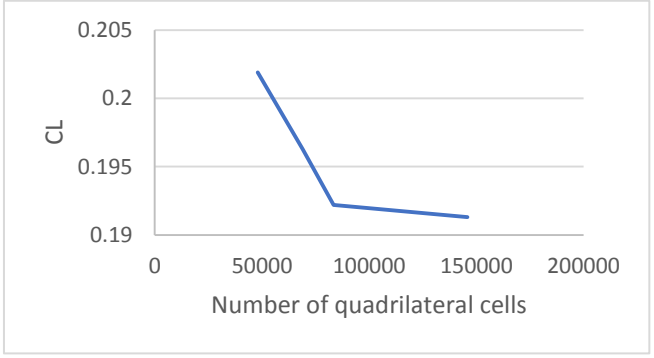

Fig: 8. *Variation of CL with number of quadrilateral cells*

Page 1-33 © MAT Journals 2018. All Rights Reserved

Boundary Conditions

A velocity of magnitude 40 m/s was applied at the inlet as velocity boundary condition whereas at exit a pressure of 1 atm was maintained as pressure outlet boundary condition. These conditions remained same for both the airfoils. Velocity boundary condition along x direction was assigned for far fields. Velocity inlet boundary condition normal to the wall was applied at secondary inlet.

Parameter Selection

In this study, values for Reynolds number of flow and free stream velocity were 5 X 10^5 and 40 m/s, respectively, and the used fluid was air. Temperature considered was 25˚C and at this temperature the density and dynamic viscosity considered were 1.177 kg/m^3 and 1.84 X 10^{-5} kg/ms respectively. In total 0 to 20˚ angles of attack were taken into consideration. The blowing ratios or blowing amplitudes (the blowing velocity (U_i) to free stream velocity (U) ratio) considered are 0 to 0.4 with an interval of 0.1 for NACA 0012 airfoil and 0 to 0.2 for LA203A. Blowing ratio is denoted by A where, A= (U_i/U).

Validation of Simulation

Validation of the simulation's dependability is very important in numerical simulation. Comparison between experimental and simulation results are shown in Fig. 9. It shows the variation of lift coefficient (C_L) with angle of attack (AOA). Experimental data were obtained at a Reynolds number of 5 × 10^5 with the smooth airfoil surfaces of NACA 0012 by Critzoz et al. [67] and the tests were conducted in the Langley low-turbulence pressure tunnel at Mach numbers no greater than 0.15 whereas the computational simulations were done at Reynolds number of 5 × 10^5 and Mach number 0.12. The results are in very good agreement from 2˚ to 8˚. Difference between the results started to appear after 8˚. These differences may be due to errors from both experiment and simulation. For example, experimental errors may be due to the inappropriate installation of airfoil model, error in taking the measurements, freestream turbulence, the interactions between wind tunnel wall and airfoil body and boundary layer. On the other hand, simulation error may be attributed to the selection of turbulence models and their various combinations with different numerical schemes, grid generation. Moreover, the limitations of two dimensional simulations can be the reasons for computational errors as two dimensional simulations cannot capture the 3D vortices and their effects. Thus, 3D simulations may produce improved results compared to 2D.

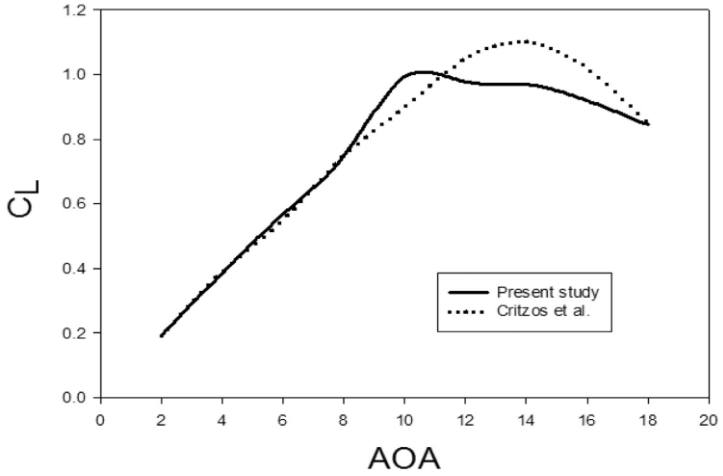

Fig: 9. *Comparative (simulation & experiment) lift curve for NACA 0012 [68]*

Page 1-33 © MAT Journals 2018. All Rights Reserved

Study of blowing on thick airfoil

This section presents the experimental setup for investigating the effect of blowing on the performance of a thick airfoil.

Experiments were conducted in a blowdown wind tunnel driven by a 75 kW backward-bladed radial blower. A schematic of the test section that produces the rotation of the wing is presented in Fig. 10. The airfoil model is firmly mounted to the circular Plexiglas windows with the axis of rotation located at the quarter-chord position.

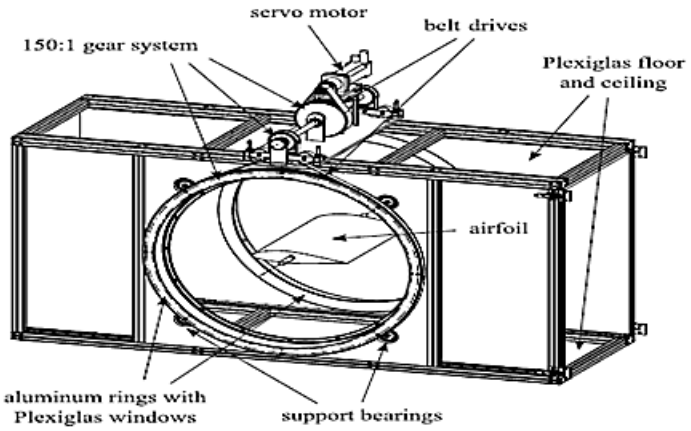

Fig: 10. *View of the test section showing the approximate location of the airfoil [69]*

The windows are rotated by means of a servo motor. Floor and ceiling of the test section were made of Plexiglas to provide access for optical measurement techniques. The constant chord NACA 0018 airfoil model with a chord length of c = 347 mm and a span of s = 610 mm was machined. A schematic of the wing showing the two control slots at 5 and 50% chord is presented in Fig. 11. The slots have a height of h = 1.2 mm and are positioned on the suction surface at positive angles of attack. The angle of the slots relative to the airfoil surface is 20 deg. It is required to minimize this angle to obtain a jet of air parallel to the wall. Pressurized air was supplied to the plenum chambers from both spanwise sides through metal flanges connected to the windows. 40 pressure ports were there in the airfoil. The vinyl tubes used to join the pressure ports to the pressure transducers. The pressurized air used for steady blowing was taken from a wall tap linked to a pressure reservoir. The outlet of the rotameter was linked to the airfoil plenum chamber by means of vinyl tubing. Whenever no control was applied, the flanges were sealed to stop a net mass flux through the slots.

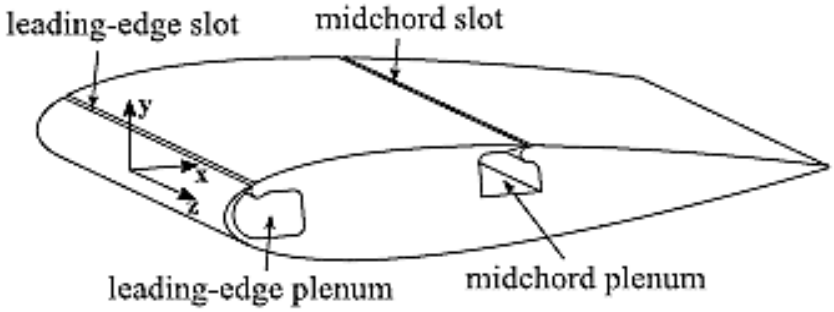

Fig: 11. *Schematic of the NACA 0018 airfoil model [69]*

Page 1-33 © MAT Journals 2018. All Rights Reserved

Study of blowing on a thick elliptical airfoil

This section contains the experimental setup for investigating the effect of blowing on the performance of a thick elliptical airfoil.

The basic elliptical airfoil (Fig. 12) has a chord of 10.86 in. and a maximum thickness-to-chord ratio of 30%. The circular arcs that form its LE and TE are 2.46 in. in diameter. The symmetry of the configuration allows tests at positive and negative incidence angles. An "I" beam rifts the interior volume of the airfoil into two independent pressure chambers. 52 static-pressure taps were there in the airfoil from which the lift and the form-drag component were calculated. Total drag was captured by traversing the wake. 15 total-pressure probes were there in the wake rake that were placed at an interval of 1 in., and two static-pressure probes located at both ends of the rake. All pressure ports were scanned electronically using Pressure Systems Inc. modules. A hot-wire anemometer was employed to calibrate the slot whenever the actuation method demanded it. The 24 in. span model was installed in a 24 x 41 in: test section of an open-loop cascade wind tunnel. To avoid laminar bubbles and strong Reynolds-number dependence, four roughness strips were used on both surfaces of the elliptical airfoil.

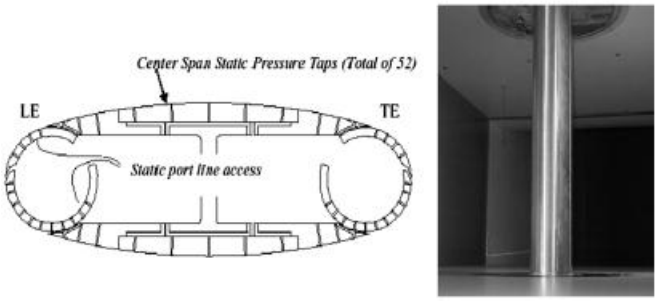

Fig: 12. *Cross section of the elliptical airfoil and its installation [70]*

A small blower could deliver up to 68 SCFM at a maximum pressure of 800 mm of water. Particle image velocimetry (PIV) was used to explain some observations made.

Study of blowing on NACA 0012 and Aerospatiale A airfoil

This section gives the governing equations that were used as well as relevant discussion on simulation setup for investigating the effect of blowing on the performance of NACA 0012 and Aerospatiale A airfoils.

Two-dimensional flow of viscous and compressible fluid is modeled by Reynolds equations (τ_{eff} - deviatoric stress tensor):

$$\frac{\partial \overline{\rho}}{\partial t} + \frac{\partial}{\partial x_j}(\overline{\rho v_j}) = 0 \tag{7}$$

$$\frac{\partial}{\partial t}(\overline{\rho v_i}) + \frac{\partial}{\partial x_j}(\overline{\rho v_i v_j}) = \rho \overline{F_i} - \frac{\partial \overline{p}}{\partial x_i} + \frac{\partial}{\partial x_j}\left[\mu\left(\frac{\partial \overline{v_i}}{\partial x_j} + \frac{\partial \overline{v_j}}{\partial x_i} - \frac{2}{3}\delta_{ij}\frac{\partial \overline{v_k}}{\partial x_k}\right)\right] + \frac{\partial}{\partial x_j}\left(-\overline{\rho v_i' v_j'}\right) \tag{8}$$

$$\frac{\partial}{\partial t}(\overline{\rho E}) + \frac{\partial}{\partial x_j}\left[(\overline{\rho E} + \overline{p})\overline{v_j}\right] = \frac{\partial}{\partial x_j}\left[\left(\lambda + \frac{c_p \mu_t}{\mathrm{Pr}_t}\right)\frac{\partial \overline{T}}{\partial x_j} + \overline{v_i}(\overline{\tau_{ij}})_{eff}\right] + S_h \tag{9}$$

Page 1-33 © MAT Journals 2018. All Rights Reserved

To close and solve this system, it is necessary to define additional equations or in some way define turbulence scales. One of the computationally simplest approaches is to use Boussinesq viscosity hypothesis:

$$-\bar{\rho}\overline{v_i' v_j'} = \mu_t\left(\frac{\partial \bar{v}_i}{\partial x_j} + \frac{\partial \bar{v}_j}{\partial x_i}\right) - \frac{2}{3}\left(\bar{\rho}k + \mu_t \frac{\partial \bar{v}_k}{\partial x_k}\right)\delta_{ij}, k = \frac{\overline{v'^2}}{2} = \frac{\overline{v_x'^2 + v_y'^2}}{2} \quad (10)$$

Turbulent viscosity μ_t is one of the flow characteristics and is determined from additional transport equations. Since no universally accepted turbulence model exists, here four different models were tried: one-equation Spalart-Allmaras (S-A), two-equation realizable k-ε (real k-ε), two-equation k-ω SST, and four-equation γ-Re_θ (trans SST).

1. Spalart-Allmaras model is a stable and reasonably accurate model for various classes of turbulent flows. It incorporates modified turbulent viscosity equation:

$$\frac{\partial}{\partial t}(\rho\tilde{\nu}) + \frac{\partial}{\partial x_j}(\rho\tilde{\nu}v_j) = G_\nu + \frac{1}{\sigma_{\tilde{\nu}}}\left[\frac{\partial}{\partial x_j}\left((\mu + \rho\tilde{\nu})\frac{\partial \tilde{\nu}}{\partial x_j}\right) + \rho C_{b2}\left(\frac{\partial \tilde{\nu}}{\partial x_j}\right)^2\right] - Y_\nu \quad (11)$$

2. Two-equation variant of k-ε model, realizable k-ε model, solves transport equations for turbulent kinetic energy k and its dissipation rate ε. There is a modified source term in the second equation:

$$\frac{\partial}{\partial t}(\rho k) + \frac{\partial}{\partial x_j}(\rho k v_j) = \frac{\partial}{\partial x_j}\left[\left(\mu + \frac{\mu_t}{\sigma_k}\right)\frac{\partial k}{\partial x_j}\right] + \mu_t S^2 - \rho\varepsilon - 2\rho\varepsilon\frac{k}{a^2} \quad (12)$$

$$\frac{\partial}{\partial t}(\rho\varepsilon) + \frac{\partial}{\partial x_j}(\rho\varepsilon v_j) = \frac{\partial}{\partial x_j}\left[\left(\mu + \frac{\mu_t}{\sigma_\varepsilon}\right)\frac{\partial \varepsilon}{\partial x_j}\right] + \rho C_1 S\varepsilon - \rho C_2\frac{\varepsilon^2}{k + \sqrt{\nu\varepsilon}} \quad (13)$$

Turbulent viscosity is computed as $\mu_t = \rho C_\mu k^2/\varepsilon$. This variant generally exceeds the standard k-ε model performance and it gives good results for complex flows.

$$\frac{\partial}{\partial t}(\rho k) + \frac{\partial}{\partial x_j}(\rho k v_j) = \frac{\partial}{\partial x_j}\left[\left(\mu + \frac{\mu_t}{\sigma_k}\right)\frac{\partial k}{\partial x_j}\right] + \mu_t S^2 - \rho\beta^* k\omega \quad (14)$$

$$\frac{\partial}{\partial t}(\rho\omega) + \frac{\partial}{\partial x_j}(\rho\omega v_j) = \frac{\partial}{\partial x_j}\left[\left(\mu + \frac{\mu_t}{\sigma_\omega}\right)\frac{\partial \omega}{\partial x_j}\right] + \frac{\alpha}{\nu_t}\mu_t S^2 - \rho\beta\omega^2 + D_\omega\left(\omega, \frac{\partial k}{\partial x_j}, \frac{\partial \omega}{\partial x_j}\right) \quad (15)$$

3. Two-equation k-ω SST model presents a combination of standard k-ω model near the walls and k-ε model in the outer layer. Transport equations for turbulent kinetic energy and its specific dissipation rate ω are:

Turbulent viscosity is computed as $\mu_t = \alpha^*\rho k/\omega$.

4. Four-equation γ-Reθ model is particularly developed for transitional flows.

Page 1-33 © MAT Journals 2018. All Rights Reserved

$$\frac{\partial}{\partial t}(\rho\gamma)+\frac{\partial}{\partial x_j}(\rho\gamma v_j)=\frac{\partial}{\partial x_j}\left[\left(\mu+\frac{\mu_t}{\sigma_\gamma}\right)\frac{\partial\gamma}{\partial x_j}\right]+P_\gamma-E_\gamma \quad (16)$$

$$\frac{\partial}{\partial t}(\rho \mathrm{Re}_{\theta t})+\frac{\partial}{\partial x_j}(\rho \mathrm{Re}_{\theta t} v_j)=\frac{\partial}{\partial x_j}\left[\sigma_{\theta t}(\mu+\mu_t)\frac{\partial \mathrm{Re}_{\theta t}}{\partial x_j}\right]+P_{\theta t} \quad (17)$$

Here the first equation determines the beginning of transition, while the second transmits the effects of outer layer flow into the boundary layer. Turbulent viscosity is computed as $\mu_t = \rho k/\omega$.

Numerical simulations were performed in ANSYS FLUENT 16.2 where finite volume method solves mass, momentum, and energy conservation equations. Fluid flow was considered as transient, and implicit density-based solver was used. Gauss-Seidel scheme solved systems of linearized equations. Least Squares Cell-Based method computed variable gradients. Spatial discretization of flow quantities was second order upwind, while temporal discretization was first order implicit. CFL number was set to 5, while the time-step order of magnitude was 10^{-3} s for airfoils and 10^{-4} s for cascades. Default values of under-relaxation factors were used.

Study of blowing on Low Re airfoil flow

This section comprises the experimental setup as well as the numerical method used for investigating the effect of blowing on low Re airfoil flow.

Experimental study

Wind tunnel set-up:

Successive experiments were carried out at a Reynolds number of 2×10^5 for pressure distributions & flow visualizations in an open-circuit wind tunnel. Besides, a closed-circuit wind tunnel is used for velocity profiles, turbulence intensities & force measurements. Tested NACA 2415 test wing has a chord of 127 mm that spans the entire width of the test section. The wing has 33 pressure tappings. The velocity profiles over the NACA 2415 airfoil were measured by using the DANTEC (55M10) constant temperature hot-wire anemometer and a computer controlled two-axis traversing mechanism. A balance system measured the aerodynamics forces. The DANTEC 55P11 normal hot-wire probe was used to measure the turbulence intensity and a 55P15 boundary layer probe was used to measure the turbulence intensity in the close circuit wind tunnel.

Fig: 13. *NACA 2415 airfoil and hot-wire anemometer set-up in the TOBB ETU low speed close circuit wind tunnel [72]*

Oil flow visualization:

Oil flow visualization is a relatively simple way of examining surface flow patterns.

Page 1-33 © MAT Journals 2018. All Rights Reserved

Fig: 14. *Oil flow visualization over NACA 2415 airfoil at 8-degree angle of attack [72]*

Numerical method

Flow Solver

The commercial RANS based code FLUENT [34] was utilized in the study of NACA 2415. In the simulations, second order upwind discretization in space is used, and the resulting system of equations is then solved using the SIMPLE coupled solution process until a convergence criteria of O(5) reduction in all dependent variable residuals is gratified. Free stream boundary conditions are employed in the upstream, downstream and outer boundaries. No-slip boundary conditions are considered at solid surfaces and transpiration boundary conditions are used at determined jet locations to simulate blowing/suction.

Turbulence models

In this study, the k–ε RNG turbulence model and the Menter k–ω SST model are applied as the standard baseline models. The k–ε RNG turbulence model is resulting from the instantaneous Navier–Stokes equations. The Menter k–ω SST model is the shear stress transport (SST) variant of the original Wilcox k–ω model.

Transition models

In this study, the k–ω SST transition model of Menter et al. and the k–kL–ω transition model of Walters and Leylek are applied. The k–ω SST transition model is based on two added transport equations beyond k and ω: the first is an intermittency equation (γ -equation) that is used to activate the transition process; and the second is the transition onset momentum thickness Reynolds number ($Re_{\theta t}$ -equation) which is forced to follow experimentally-determined correlations with some lag. The k–kL–ω model is considered as a three-equation eddy viscosity type, which contains transport equations for turbulent kinetic energy (k), laminar kinetic energy (kL), and specific dissipation rate (ω).

As for the the wall boundary conditions, the k–kL–ω transition model uses a Neumann type boundary condition which specifies the normal derivative of the function on a surface, whereas the k–ω SST transition model uses Dirichlet type wall boundary conditions which gives the value of the function on a surface.

Page 1-33 © MAT Journals 2018. All Rights Reserved

Solution grid

A C-type structured grid applied for the single airfoil is produced by the GAMBIT program. The grid extends from −10 chords upstream to 20 chords downstream and the upper and lower boundary extends 10 chords from the profile. The wall coordinate y+ of the first grid point off the body is confirmed to be less than 1. In this study, different sized grids with 25,000, 35,000 and 45,000 nodes were used to ensure grid independence of the calculated results. The grid size giving a grid independent result was designated to be 35,000.

RESULTS AND DISCUSSIONS

Study of blowing on NACA 0012 and LA203A airfoils

This section investigates the effect of blowing on the performance of a symmetric airfoil (NACA 0012) and high lift airfoil (LA203A). First the results of simulation of symmetric airfoil is presented which is followed by the discussion of the results of LA203A airfoil.

Simulation Results of NACA 0012 At blowing amplitude 0.1

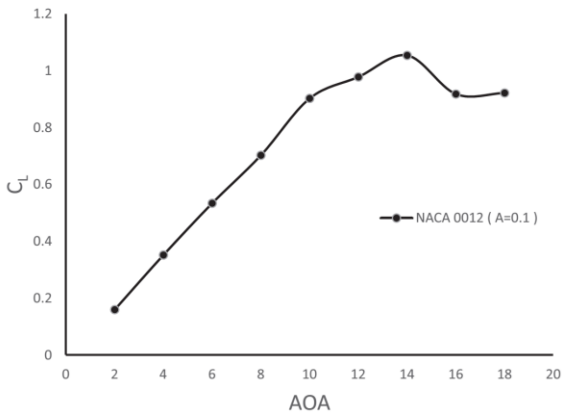

Fig: 15. *Variation of C_L with AOA at A=0.1 for NACA 0012 [68]*

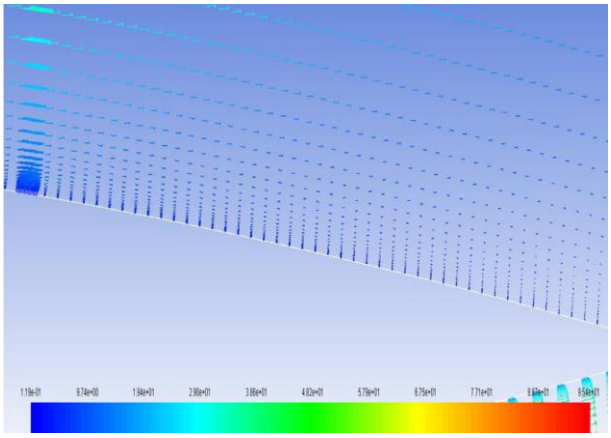

Fig: 16. *Velocity vectors at AOA=14˚ & A=0.1 for NACA 0012 [68]*

Fig. 15 shows how the lift coefficients vary with the variation of angle of attack.

As the velocity of the injected air is only 10% of the free stream air so this secondary air does not obstruct the free stream air (as also seen from Fig. 16) rather the resultant velocity increases. As the velocity increases, pressure decreases on upper surface which gives greater pressure difference (with respect to lower surface). Due to this increase in pressure difference, lift increases which is shown by the graph at Fig. 10.

From the perspective of momentum conservation: as more air in injected and this increases the resultant velocity which increases the net downward momentum acting on the airfoil, so to balance it there will be an increase in upward momentum which will cause an increase in lift.

From the perspective of energy conservation: As the secondary air injected through blowing increases the resultant velocity so the total kinetic energy will increase for which the pressure energy will decrease which will increase the difference in pressure energy resulting a rise in lift.

It is also observed that that the blowing air will keep the flow more attached to the surface which will delay the flow separation because of which the stalling angle of attack increases by 4 degrees.

Page 1-33 © MAT Journals 2018. All Rights Reserved

At blowing amplitude 0.2

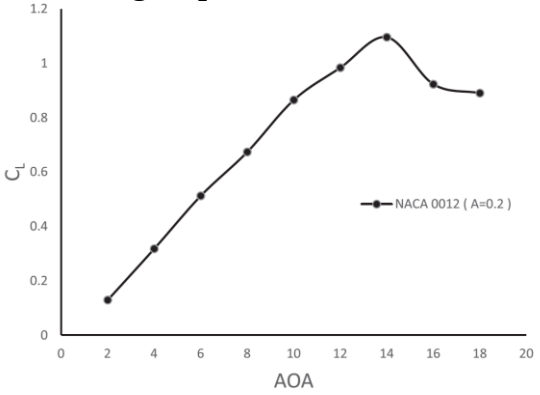

Fig: 17. *Variation of C_L with AOA at A=0.2 for NACA 0012 [68]*

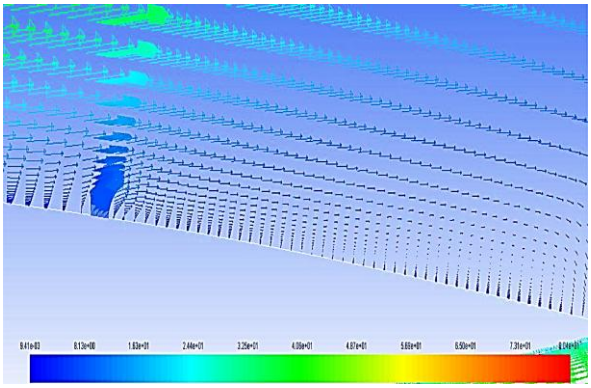

Fig: 18. *Velocity vectors at AOA=14˚ & A=0.2 for NACA 0012 [68]*

Fig. 17 shows the lift curve for NACA 0012 at an amplitude of 0.2. The lift coefficient has increased by 4% whereas the stalling angle of attack is remaining same.

In this case also the blowing air is not causing any change in direction of the free stream air and hence it increases the resultant velocity. As this time the blowing air velocity is more than the previous case so the decrease in pressure will also more and subsequently the pressure difference is also more which will cause more increment in lift.

Like the previous case, according to momentum conservation: there will be a net increase in downward momentum and subsequently a greater upward momentum will be required to balance it and this increased upward momentum will cause augmentation of lift.

Similarly, it can be explained by energy conservation: as blowing ratio increases so the kinetic energy increases as a result pressure energy decreases. This causes a rise in the difference of pressure energy which acts in upward direction causing lift to increase.

At blowing amplitude 0.3

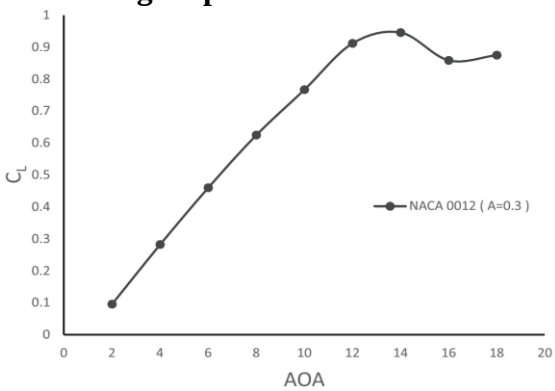

Fig: 19. *Variation of C_L with AOA at A=0.3 for NACA 0012 [68]*

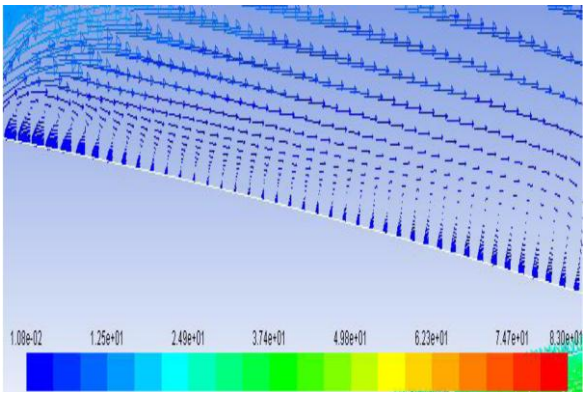

Fig: 20. *Velocity vectors at AOA=14˚ & A=0.3 for NACA 0012 [68]*

Fig. 19 represents the lift curve when the secondary blowing velocity is 30 percent of the free stream velocity. In this case, at 60% of chord length from leading edge the secondary fluid is injected at a velocity of 12 m/s.

The velocity of the blowing air is large enough to cause obstruction to the free stream air (as seen from Fig. 20). Thus, the flow area increases, according to

Page 1-33 © MAT Journals 2018. All Rights Reserved

continuity equation the resultant velocity in downward direction decreases which increases the pressure on upper surface. It reduces the pressure difference between upper and lower surfaces for which the lift decreases.

As the resultant velocity in the downward direction decreases so the net momentum acting downward decreases to balance which a lesser upward momentum is enough. Hence the lift decreases.

From the energy conservation point of view: even though the blowing ratio increases which means the blowing air velocity has increased and it appears that the kinetic energy is supposed to increase but, it does not happen. Because the blowing air now contributes in formation of vortices and as a result it cannot increase the net kinetic energy in downward direction unlike to the previous cases. This results in loss of kinetic energy which gives rise in pressure energy of the upper surface. Hence the pressure energy difference between the two surfaces decrease which causes drop in lift.

But, as the blowing air keeps the air on the upper surface attached to it so the stalling angle remains same.

At blowing amplitude 0.4

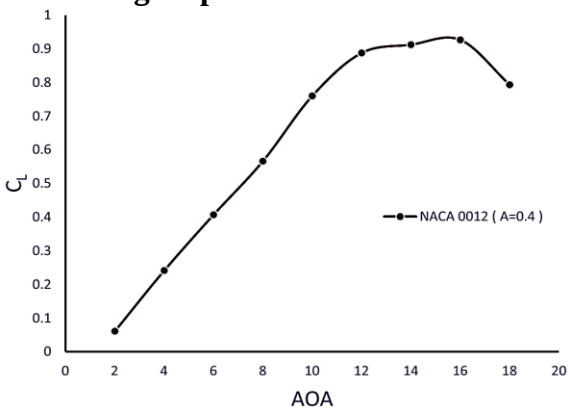

Fig: 21. *Variation of C_L with AOA at A=0.4 for NACA 0012 [68]*

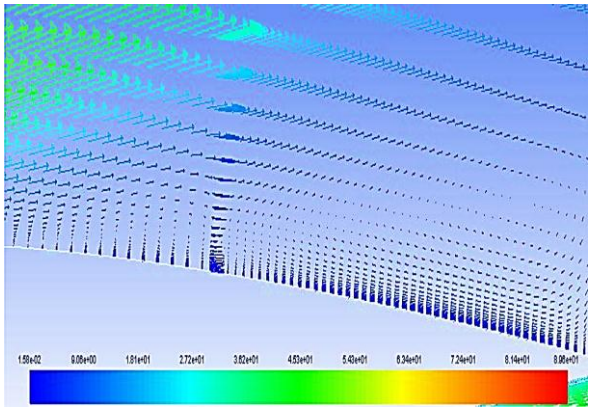

Fig: 22. *Velocity vectors at AOA=14˚ & A=0.4 for NACA 0012 [68]*

Fig. 21 shows that there is an increment in stalling angle of attack with a decrement in the maximum lift coefficient.

As the blowing ratio in this case is greater than the previous case so the obstruction caused by the blowing air is also greater (as seen from Fig. 22). As a result, lift is also affected in a greater extent.

The similar explanation (as stated above) from the perspective of mass, momentum and energy conservation is applicable for this case also but with a greater effect as a result lift decreases more in this case.

Even though the secondary air injected through blowing does not enhance the lift but it causes additional vortices to form (as result vortices form in both upstream and downstream which can be observed from right part of Fig. 29) which keeps the flow attached to the surface longer. It has caused further delay in flow separation leading to 2-degree gain in stalling angle.

Page 1-33 © MAT Journals 2018. All Rights Reserved

Simulation Results of LA203A
At blowing amplitude 0 (without blowing)

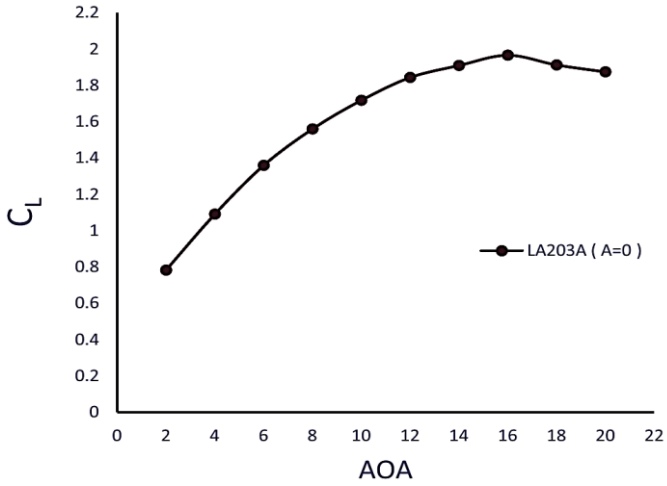

Fig: 23. *Variation of C_L with AOA at A=0 for LA203A [68]*

Fig. 23 represents lift curve for LA203A without blowing. This shows that this airfoil stalls at 16° with a corresponding maximum lift coefficient of 1.9671.

At blowing amplitude 0.1

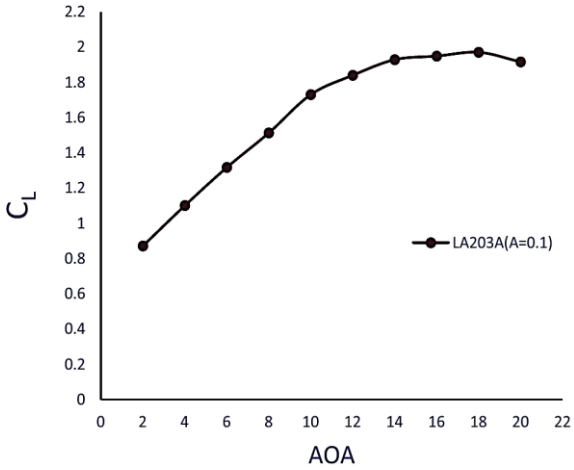

Fig: 24. *Variation of C_L with AOA at A=0.1 for LA203A [68]*

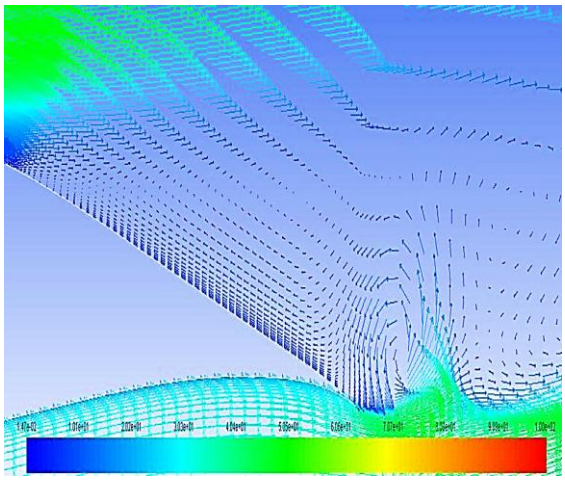

Fig: 25. *Velocity vectors at AOA=14˚ & A=0.1 for LA203A [68]*

Fig. 24 represents the change in lift coefficient with change in angle of attack for LA203A airfoil when the blowing velocity is 10% of the main free stream velocity. In this case, gain is accomplished from both the perspective of maximum angle of attack (increased by 2° from 16° to 18°) as well as maximum lift coefficient (increased by .17% from 1.9671 to 1.9705).
Both are due to the formation of vortices due to the introduction of secondary flow. But as the point of separation is behind the point of injection that is why blowing has less effect on increment in maximum lift coefficient.

Additional air injected through blowing increases resultant velocity of the flow so the pressure decreases. It increases the pressure difference which causes the lift to increase.

Page 1-33 © MAT Journals 2018. All Rights Reserved

According to the principle of momentum conservation: as the additional momentum is injected through blowing so the total downward momentum increases to balance which the upward momentum increases which can be considered as an increase in lift.

According to energy conservation principle: as additional air is injected with additional velocity so the kinetic energy increases and pressure energy decreases. It increases the difference in pressure energy between the two surfaces of the airfoil which ultimately increases lift.

As additional injected air helps to keep the flow more attached to the surface compared to the case of no blowing so the stalling angle increases.

At blowing amplitude 0.2

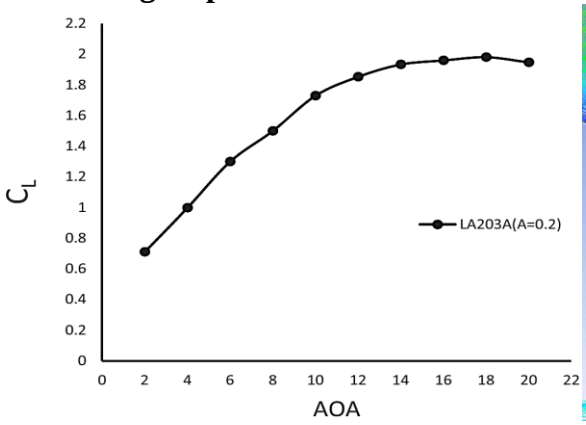

Fig: 26. *Variation of C_L with AOA at A=0.2 for LA203A [68]*

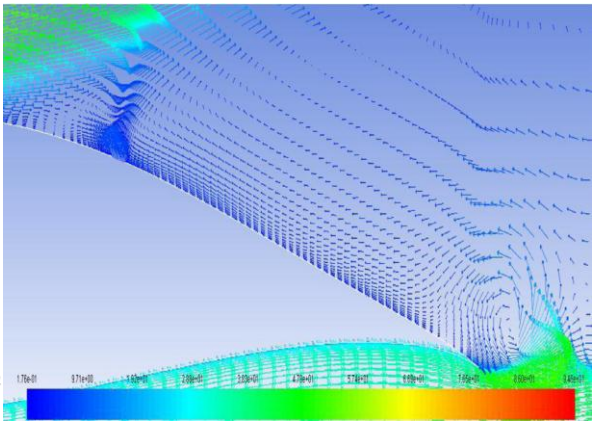

Fig: 27. *Velocity vectors at AOA=14˚ & A=0.2 for LA203A [68]*

Fig. 26 shows that, at an amplitude 0.2, the lift coefficient has increased by .71% which is much greater than the increment of lift coefficient in previous case. But the change in stall angle is very small (almost negligible).

In this case, mass, momentum and energy conservation principles can be applied in a likely way to the previous case which causes similar effect on lift (that is the lift increases in this case also).

In summary, this study analyzed the effect of blowing on the performance of NACA 0012 and LA203A airfoils. For measuring the aerodynamic performance, lift curves were used from which two types of conclusion can be drawn: one in terms of maximum lift coefficient and the other in terms of maximum angle of attack.

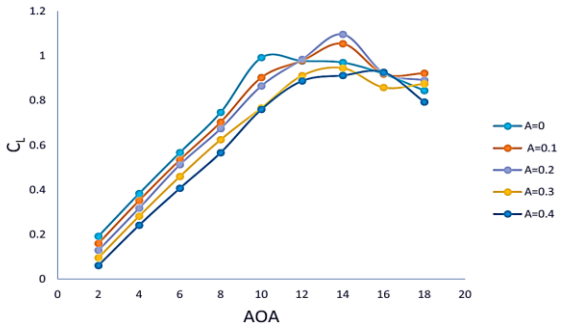

Fig: 28. *Variation of C_L with AOA for NACA 0012 [68]*

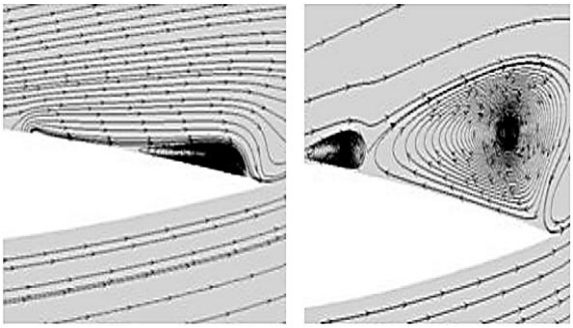

Fig: 29. *Streamline patterns at AOA=14˚ (A=0.2) & at AOA=16˚ (A=0.4) for NACA 0012 [68]*

Page 1-33 © MAT Journals 2018. All Rights Reserved

Comparative lift curves (Fig. 28) at all amplitudes for NACA 0012 shows that maximum lift coefficient is achieved at an amplitude of 0.2 whereas the maximum angle of attack is achieved at an amplitude of 0.4. This means, for maximum lift coefficient there is an optimum amplitude beyond which it starts to fall or in other word only at which the maximum value is attained whereas for stalling angle of attack: it increases with the increase in amplitude. As optimum value of two parameters were found at two different amplitude so streamline patterns of these two cases are presented which will help to understand the underlying reason behind such changes in aerodynamic performance. Left part of Fig. 29 shows that the flow over the airfoil surface at A=0.2 is much more streamlined compared to the case of A=0.4 (right part of Fig. 29). So, the downward momentum is greater in case of A=0.2 compared to the case of A= 0.4. To balance momentum, the airfoil in case of A=0.2 gives more upward momentum than the case of A=0.2. Thus, the lift is greater in case of A=0.2. On the other hand, even though the flow is not that much streamlined compared to the case A=0.2 but still the flow is attached with the upper surface of the airfoil which is causing the delay in stall. Again, Fig. 29 shows that in addition to the formation of vortices at upstream, some vortices are also formed at downstream which is further delaying the stall causing a gain in maximum angle of attack.

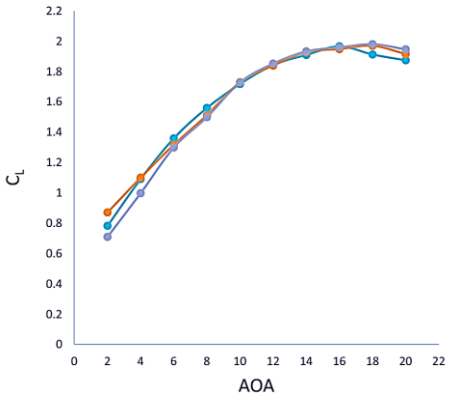

Fig: 30. *Variation of C_L with AOA for LA203A [68]*

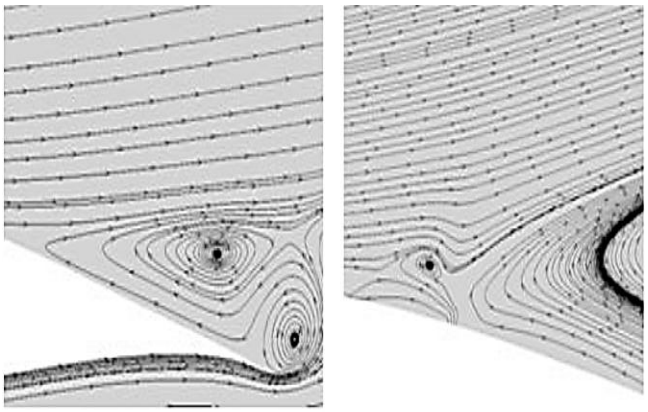

Fig: 31. *Streamline patterns at AOA=18˚ at A=0.1 and A=0.2 for LA203A [68]*

Combined lift curves for LA203A airfoil at amplitude 0.1 and 0.2 (Fig. 30), shows that, the introduction of blowing has increased both the maximum lift coefficient (increased to 1.9812) as well as the stalling angle (increased to 18˚) of attack. The corresponding streamline pattern is shown in Fig. 31. It shows that, at A=0.1, vortices form near the trailing edge only whereas in case of A=0.2, vortices are generated near leading edge in addition to the trailing edge vortices. These causes delay in flow separation as well as increment in maximum lift coefficient.

So, for both NACA 0012 and LA203A airfoils performance gain is achieved through applying blowing with a difference that, for NACA 0012 there is an optimum blowing ratio (A=0.2) beyond which maximum lift coefficient drops which does not occur in case of LA203A airfoil. But same type of conclusions can be drawn for both the airfoils from the perspective of stalling angle of attack and that is with the increment of blowing amplitude, stalling angle of attack increases.

Page 1-33 © MAT Journals 2018. All Rights Reserved

Study of blowing on thick airfoil

This section examines the effect of blowing on the performance of a thick airfoil.

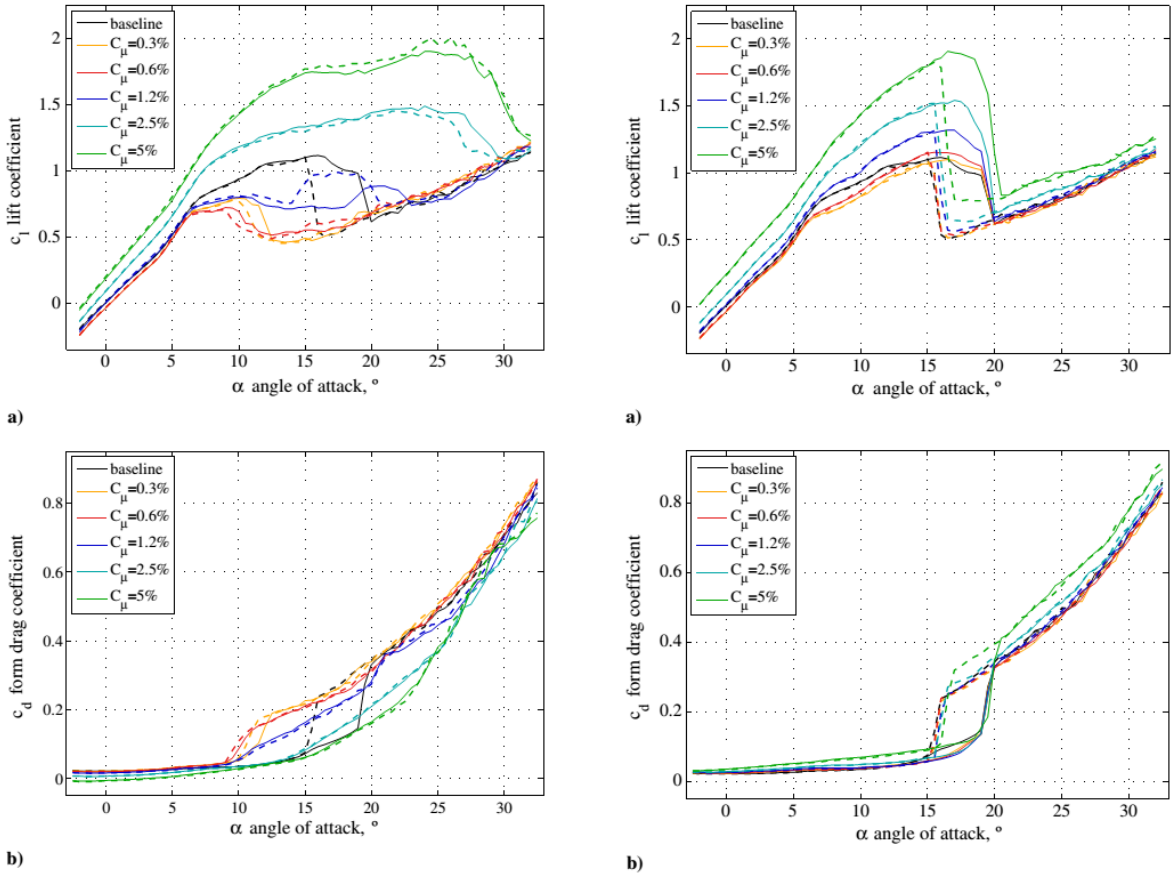

Fig: 32. *Control from the leading-edge slot (x/**c** = 5%) & Control from the mid-chord slot (x/**c** = 50%) [69]*

Fig. 32 shows the effect of momentum coefficient on the performance of NACA 00018 airfoil in terms of lift coefficient and drag coefficient for two different slot locations.

For both locations, as the moment coefficient increases the lift curve goes up. This is because as the moment coefficient increases it allows more blowing air to be injected which increases the momentum acting in downward direction. As total downward momentum increases so according to momentum conservation total upward momentum must increase as a result lift increases.

From energy conservation perspective: as the kinetic energy on upper surface of the airfoil increases so the pressure energy decreases and the difference between the pressure energy between two surfaces increase and hence the lift increases.

The drag curve at the location 50% shows that changing of moment coefficient has little effect on drag coefficient as all the curves are almost close to each other.

But the drag curve at location 5% shows that there is effect of moment coefficient on the drag curve of the airfoil and that is drag decreases at higher moment coefficients and increases at lower coefficients. As in this case blowing slot is located at the leading edge which is far away from the separation point (compared to that of the slot location at 50%), so enough momentum is required to be injected for reduction in drag. Because if

Page 1-33 © MAT Journals 2018. All Rights Reserved

the amount of injected momentum is less then it will not be sufficient to eliminate or reduce the vortices that form near separation point.

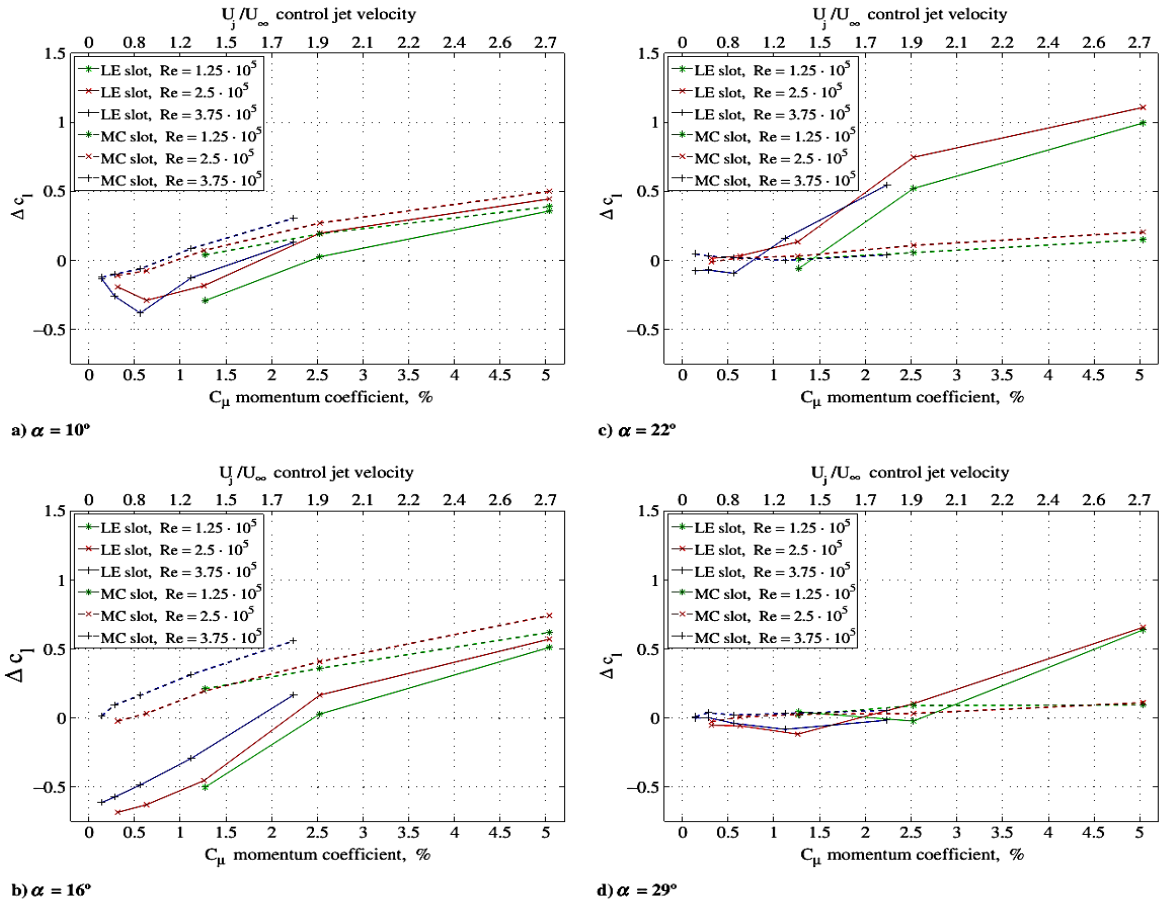

Fig: 33. *Change in lift coefficient Δ* ***cl*** *produced with control during quasi-static pitch-up. [69]*

Fig. 33 shows the effect of location of blowing slot on the variation of lift coefficient with respect to moment coefficient at four different angles of attack (two lower angles and two higher angles) at different Reynolds number. These also show the effect of blowing ratio on the change in lift coefficient.

In general, at all angles of attack it is observed that as the moment coefficient increases the lift coefficient increases thus the change in lift coefficient increases. It is due to the fact what is just explained for the immediate previous set of graphs (i.e., as the momentum coefficient increases the momentum injection increases which increases the net downward momentum to balance which the net upward momentum increases as a result lift increases.)

From the graphs of comparatively lower angles of attack (i.e., at 10 degrees and 16 degrees): it is observed that the mid chord slots give better lift coefficient than the leading-edge slot. It is since at comparatively lower angles of attack flow remain more attached to the airfoil upper surface that is flow get separated after the mid chord not before that. So, setting the blowing location just before the separation point is much more effective than the leading-edge slot and it has better control over flow separation.

Page 1-33 © MAT Journals 2018. All Rights Reserved

On the other hand, the graphs of comparatively higher angles of attack (i.e., at 22 degrees and 29 degrees) show that the better performance can be achieved with leading edge slots. As at higher angles of attack the flow remain less attaches to the airfoil surface compared to the lower angles of attack so the separation point is often found around or before the midchord. That is why leading-edge slot before the separation point has better control over the separation at high angles of attack compared to midchord slots. Hence the change in is more lift coefficient for leading edge slots at higher angles of attack.

In general, in almost all cases, as the blowing ratio increases the change in lift coefficient increases. And it is obvious since increase in blowing ratio will increase the injected air velocity which will increase the momentum. According to momentum conservation, to balance the increased downward momentum a greater upward momentum is generated which gives rise in the change in lift coefficient.

Study of blowing on a thick elliptical airfoil

This section inspects the effect of blowing on the performance of a thick elliptical airfoil.

Blowing Upstream of the Separation Location Near the TE (i.e., Slot Located at 90 deg)

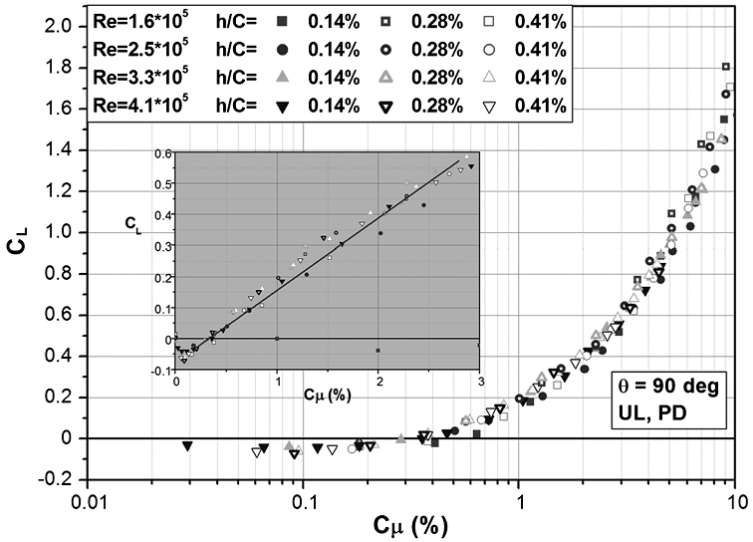

Fig: 34. *Dependence of CL on Cμ [70]*

Fig. 34 shows the effect of steady momentum coefficient and slot width on lift coefficient. It depicts that as the steady momentum coefficient increases, lift coefficient increases. As steady momentum coefficient increases blowing velocity increases which increases the resultant velocity over the upper surface of the flow thus pressure decreases. So, the pressure difference which is acting in upward direction increases as a result lift increases.

Again, increases blowing ratio gives increases momentum that is net downward momentum acting in downward direction increases to balance which upward momentum increases which results in increase in lift.

From the perspective of energy conservation: as steady momentum coefficient increases so the blowing velocity increases and the kinetic energy increases and pressure energy decreases. The difference between the pressure

Page 1-33 © MAT Journals 2018. All Rights Reserved

energies increases which give a push in upward direction increasing lift.

This trend remains almost same at four different Reynolds number and slot widths. But effect of slot width will be more pronounced which will be shown in another figure which will contain a wider range of slot widths.

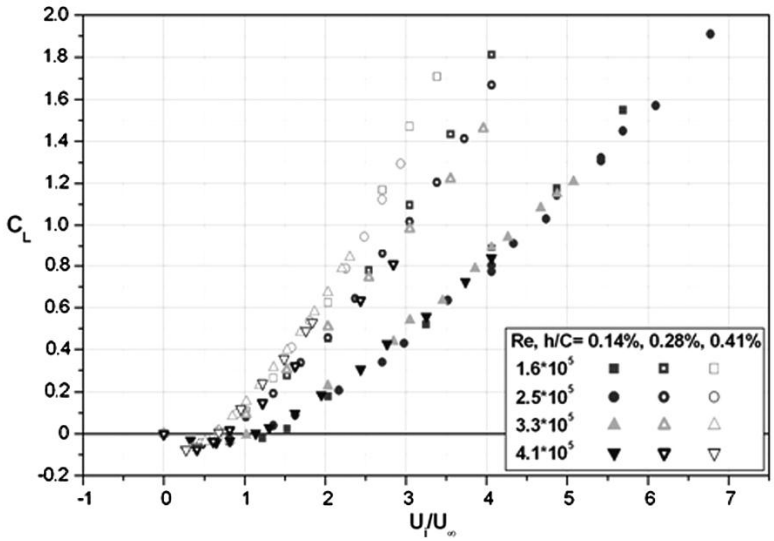

Fig: 35. *Effect of blowing ratio on lift [70]*

Fig. 35 shows the effect of blowing ratio on the performance of lift coefficient. It shows that lift increases with the increase in blowing ratio.

The reasons are almost same as it is explained for the previous figure. This case also it is observed for four different Reynolds number and same trend is achieved.

But, additionally this graph clearly shows the effect of slot width on lift coefficient. As the slot width increases lift increases more sharply. This is because, with the increment in the width of the slot the mass injection increases as a result momentum increases. As the downward momentum acting on airfoil increases so to balance it the net upward momentum also increases which ultimately causes increase in lift.

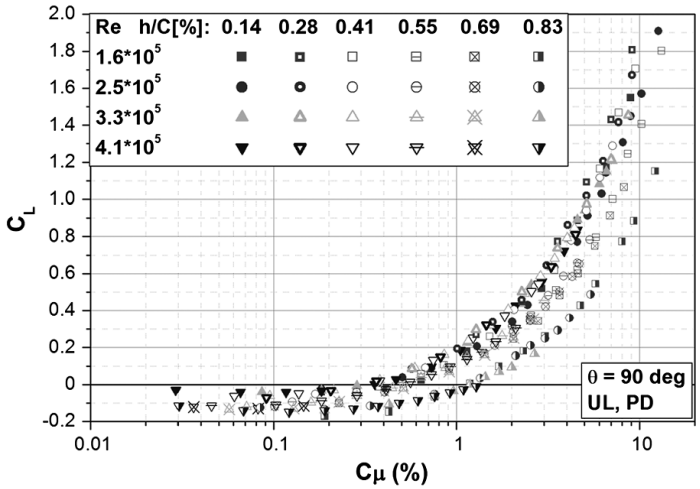

Fig: 36. *Dependence of CL on Cμ for a wider range of slot widths [70]*

Page 1-33 © MAT Journals 2018. All Rights Reserved

This Fig. 36 represents the total picture of the effect of slot width on the lift coefficient. It is observed that beyond slot width to chord ratio 0.41, lift decreases with the increase in slot width. This shows that there remains an optimum slot width beyond which performance of airfoil deteriorates in terms of lift. Because beyond that optimum slot width, if it is increases the amount of air that is injected starts obstructing the main stream air and hence instead of giving positive effect on lift in starts giving negative effect. Because due to creation of obstruction there will be momentum loss which will reduce the net downward momentum acting downward direction as a result to balance it less upward momentum will be sufficient which results in decrease in lift.

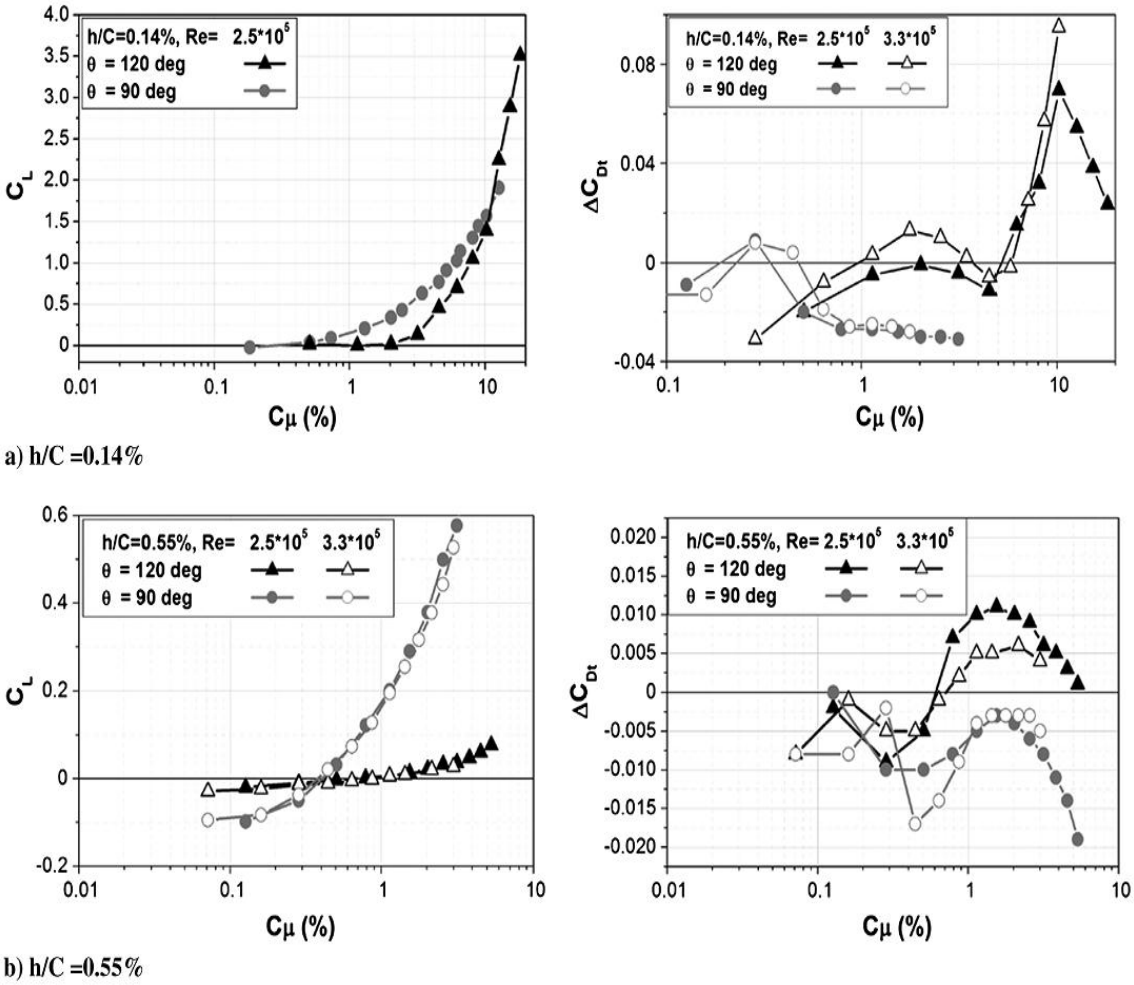

Fig: 37. *Blowing through slots of 90 and 120 degree from TE at 0 degree [70]*

Fig. 37 represents the effect of blowing angle on airfoil performance both in terms of lift and drag coefficient in two cases of slot width ratios and two Reynolds number. In all cases it is observed that as blowing angle is changed from 90 degrees to 120-degree lift decreases and drag increases that the overall performance of airfoil decreases.

It is because at 120 degree the blowing air flowing opposite to the main stream of air which clearly obstructs the flow. Thus, it affects the performance of airfoil negatively.

Page 1-33 © MAT Journals 2018. All Rights Reserved

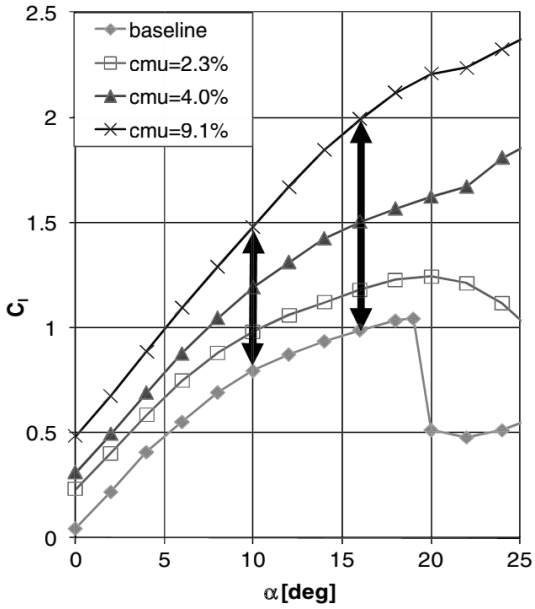

Fig: 38. *Effect of Cμ on lift curve [70]*

Fig. 38 clearly shows the effect of steady momentum coefficient on lift curve. It demonstrates that as the momentum coefficient increases lift curve goes upward that is lift increases.

It is since as steady momentum coefficient increases the net downward momentum acting on airfoil increases to balance which the net upward momentum must increase which results in increment of lift.

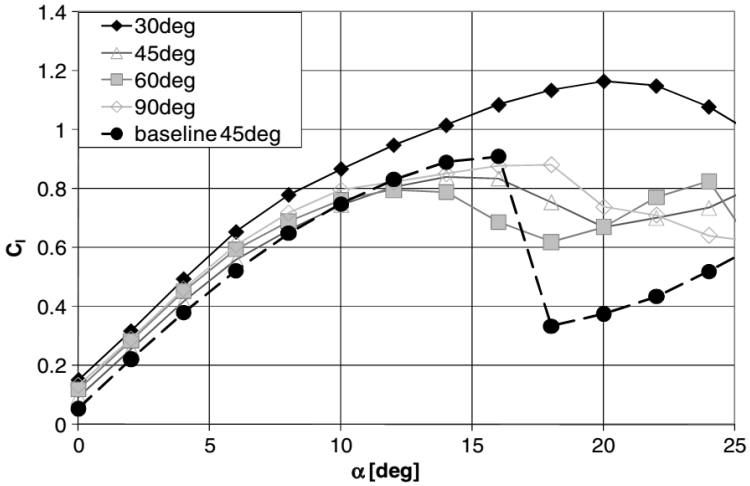

Fig: 39. *Effect of on CL at Re 250**;** 000; LE actuation h/C **=0.**28 %; Cμ = 1:8 %. [70]*

Fig. 39 clearly depicts the effect of blowing angle on lift curve. It is evident from the figure that the best performance is achieved at an angle 30 degree and at higher angles the lift curve drops.

It is because at lower blowing angle the injected flow through blowing remain more inline with the main stream of that is why the best performance is achieved and vice versa. As a result, best performance is achieved at lower blowing angle.

Study of blowing on NACA 0012 and Aerospatiale A airfoil

This section examines the effect of blowing on the performance of NACA 0012 airfoil and Aerospatiale A airfoil. In

Page 1-33 © MAT Journals 2018. All Rights Reserved

addition to that it also studies the effect of blowing on turbomachinery (namely compressor and turbine).

First the results of simulation of NACA 0012 airfoil are presented which is followed by the discussion of the results of Aerospatiale A airfoil. Then the results on turbomachinery are presented.

Table: 2. *Lift coefficient Cl for Aerospatiale A [71]*

D_j/c	$B = 0$	$B = 0.5$	$B = 1$	$B = 2$
0.25%	1.578	1.557	1.704	1.929
0.5%	1.578	1.509	1.665	1.951
1%	1.578	1.367	1.394	1.805

Table: 3. *Drag coefficient Cd for Aerospatiale A [71]*

D_j/c	$B = 0$	$B = 0.5$	$B = 1$	$B = 2$
0.25%	0.0189	0.0178	0.0190	0.0188
0.5%	0.0189	0.0169	0.0152	0.0096
1%	0.0189	0.0104	0.0021	-0.011

These tables represent the variation lift and drag coefficient with respect to blowing ratio at three different jet diameters for Aerospatiale A airfoil at 13-degree angle of attack.

It is evident that blowing effectively increases the lift coefficient. At higher blowing ratio the higher lift coefficients are achieved. This is because blowing essentially injects momentum to the airfoil upper surface increasing net downward acting momentum whereas to balance it greater upward momentum is required which gives rise in lift coefficient. Irrespective of jet diameter, at higher blowing ratios the lift coefficients are greater.

For drag coefficient, it will only decrease when the jet diameter increases. At all nonzero blowing ratios drag decreases with the increment of jet diameter. Because, with the increment of jet diameter more air can be injected which can better reduce the effect of vortices causing decrease in drag.

Table: 4. *Lift coefficient Cl for NACA 0012 [71]*

D_j/c	$B = 0$	$B = 0.5$	$B = 1$	$B = 2$
0.25%	0.270	0.277	0.403	0.858
0.5%	0.270	0.182	0.420	0.953
1%	0.270	0.038	0.057	1.031

Table: 5. *Drag coefficient Cd for NACA 0012[71]*

D_j/c	$B = 0$	$B = 0.5$	$B = 1$	$B = 2$
0.25%	0.0565	0.0520	0.0628	0.1143
0.5%	0.0565	0.0418	0.0612	0.1274
1%	0.0565	0.0285	0.0310	0.1395

These tables represent the variation lift and drag coefficient with respect to blowing ratio at three different jet diameters for NACA 0012 airfoil at 4-degree angle of attack.

Like the previous case in this case also, lift coefficient increases with the increase in blowing ratio for same reason as stated above.

For drag coefficient, as the jet diameter increases the drag coefficient decreases except the blowing ratio 2. The explanation stated just for the previous tables is also generally applicable here also. At blowing ratio 2, secondary injected flow starts to cause obstruction the main free stream which results in increase in drag coefficient

Page 1-33 © MAT Journals 2018. All Rights Reserved

Table: 6. *Δ prel for compressor cascade [71]*

D_j/c	$B = 0$	$B = 0.5$	$B = 1$	$B = 2$
0.25%	–0.52	–0.49	–0.56	–0.62
0.5%	–0.52	–0.46	–0.54	–0.63
1%	–0.52	–0.41	–0.50	–0.64

Table: 7. *Δ prel for turbine cascade [71]*

D_j/c	$B = 0$	$B = 0.5$	$B = 1$	$B = 2$
0.25%	9.57	9.00	9.94	11.17
0.5%	9.57	8.91	10.04	11.64
1%	9.57	8.84	9.93	12.20

These tables represent the variation in pressure difference with respect to jet diameter and blowing ratio. As the blowing ratio increases, the magnitude of pressure difference increases in both case of compressor and turbine. Because, with increase in blowing more air is injected with greater velocity so pressure decreases and the difference in pressure increases.

As the jet diameter increases, at lower blowing ratio (0.5 and 1) the magnitude of pressure difference decreases which applicable for both compressor and turbine with an exception that at 0.5% of jet diameter to chord ratio pressure difference increases.

On the other hand, at higher blowing ratio (2), the magnitude of pressure difference increases which is applicable for both compressor and turbine. It is because, sufficient momentum is required to be injected to get a beneficial effect from turbomachinery (compressor and turbine cascade) which can be attained only at higher blowing ratio.

Study of blowing on Low Re airfoil flow

This section investigates the effect of blowing on low Re airfoil flow.

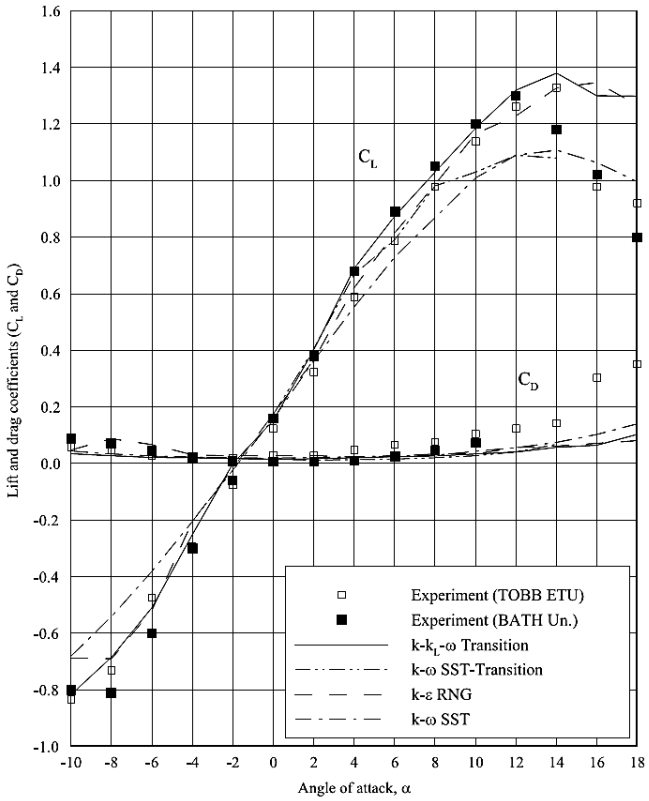

Fig: 40. *Experimental and numerical lift and drag coefficients of the NACA 2415 at Re = 2 × 10^5 [72]*

Page 1-33 © MAT Journals 2018. All Rights Reserved

This graph of Fig. 40, shows how close the values of lift and drag curves of simulation to that of experiment.

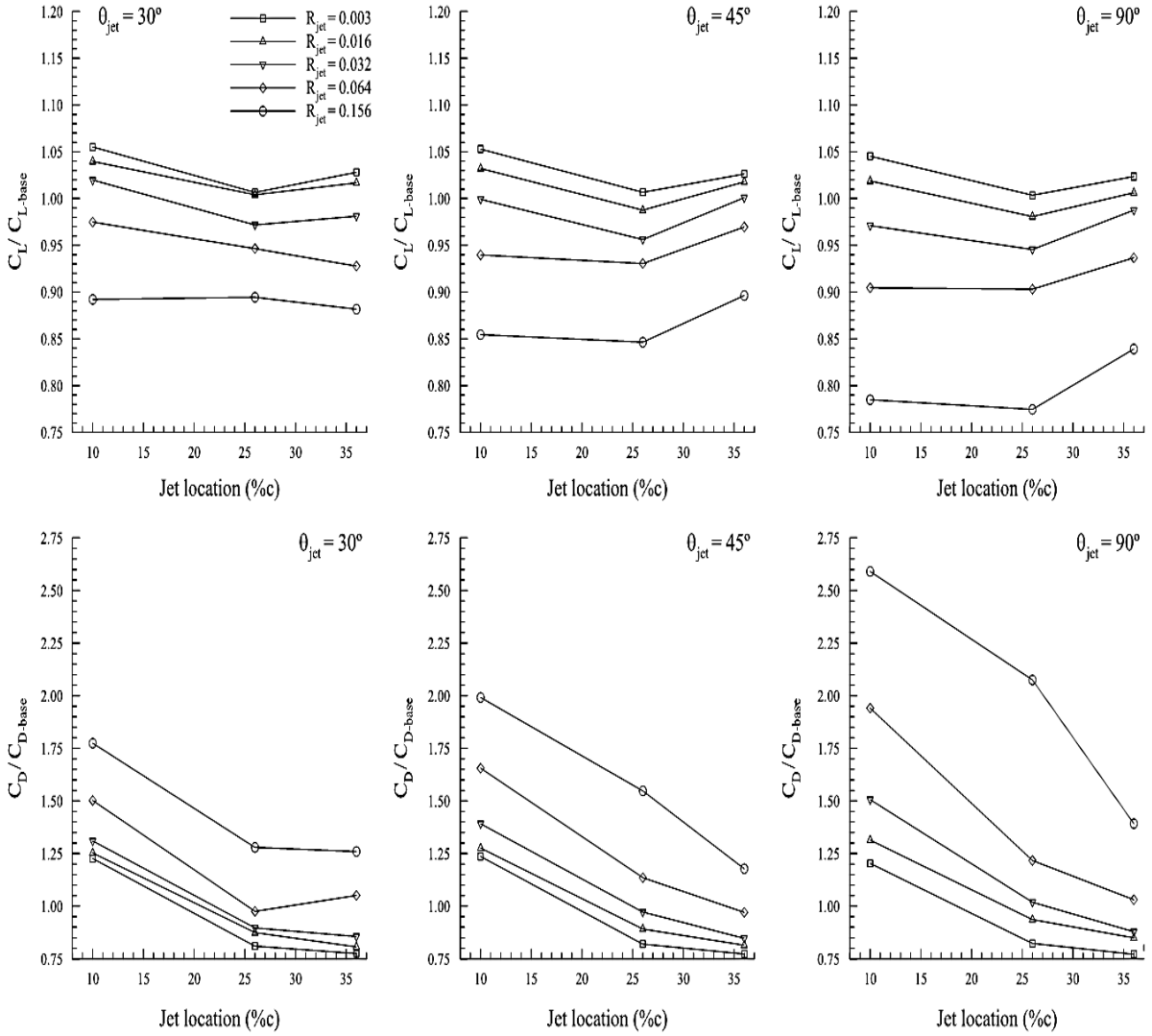

Fig: 41. *C_L and C_D coefficients of NACA 2415 airfoil at α = 8° with blowing using the k–k_L–ω transition model [72]*

Three graphs of the first row (of Fig. 41) show the effect of blowing ratio on the variation of lift ratio with respect to jet location at three different blowing angles. The same for drag ratio is presented in the graphs of second row.

It is observed that at low Reynolds number, as the blowing ratio increases the lift coefficient decreases and drag coefficient increases for all jet locations and all the three-blowing angle which is opposite the cases of high Reynolds number. It is because at the low Reynolds number, smaller injection of momentum will be sufficient to cause the flow more attached to the surface increasing the effective downward momentum. To balance this the upward momentum will increase.

At higher blowing ratio, even though the more air will be injected as the velocity increases but at low Reynolds number they will contribute in formation of vortices causing loss in momentum. This will result in loss of lift and increase in drag.

Page 1-33 © MAT Journals 2018. All Rights Reserved

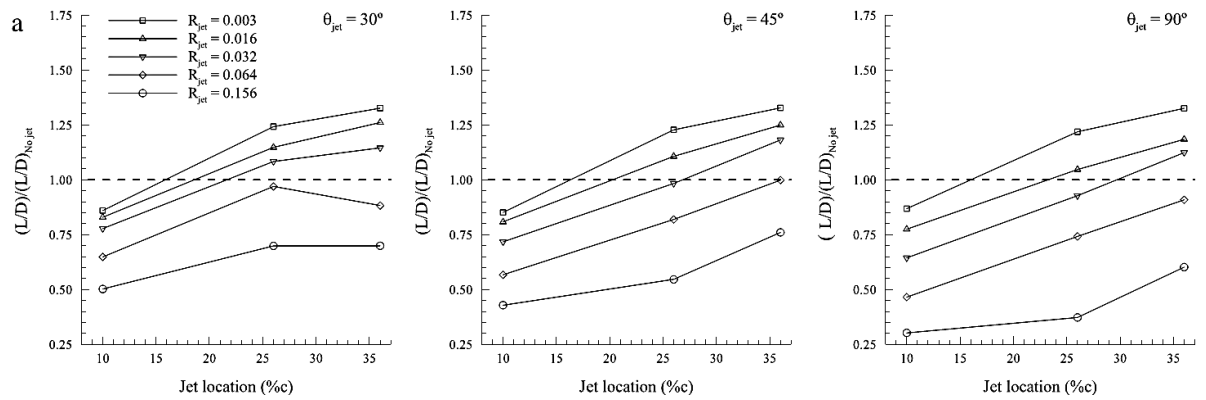

Fig: 42. *L/D ratios of NACA 2415 airfoil at α = 8° with (a) blowing using the k–kL–ω transition model [72]*

These graphs (of Fig. 42) show the effect of blowing ratio on the variation of lift to drag ratio with respect to jet location. From these graphs it becomes clear that as the blowing ratio increases lift to drag ratio decreases. The fact which is explained just before this set of graphs, it is similarly applicable for this case also. This trend is same at all blowing angles.

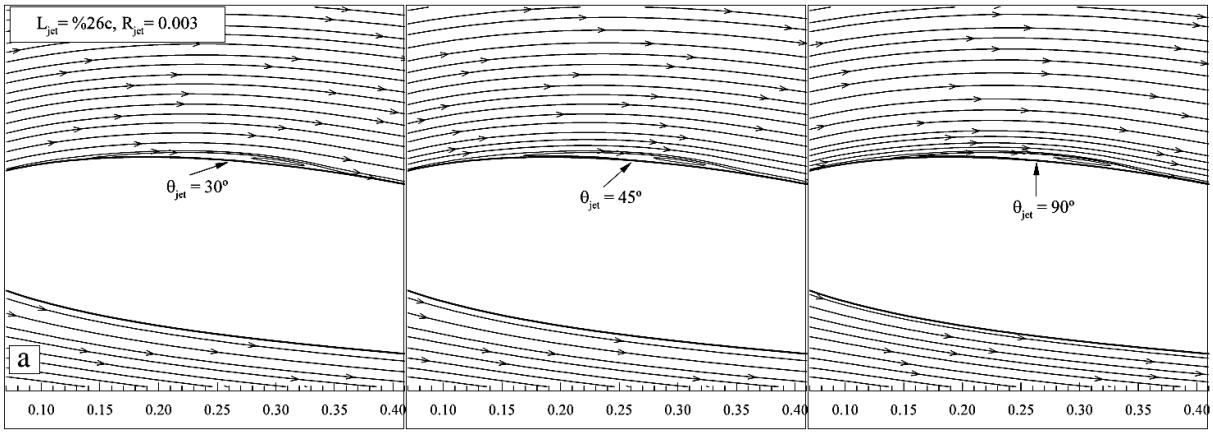

Fig: 43. *Streamlines of NACA 2415 airfoil at α = 8° with (a) blowing for Rjet = 0.003 at Ljet = 0.26c with different jet angles using the k–kL–ω transition model [72]*
This figure (Fig. 43) show streamlines at various blowing angles.

CONCLUSION

The use of blowing for lift enhancement is a convenient way as the compressed air is readily available on airborne vehicles. But only having the knowledge about the appropriate effect of various blowing parameters on the performance of airfoil will lead to meaningful application of this flow control strategy. And this study reveals some such effects.

The study on NACA 0012 and LA203A airfoils show that for NACA 0012 there is an optimum blowing amplitude or blowing ratio (0.2) beyond which the maximum lift coefficient decreases with the increase of blowing ratio whereas the higher stalling angle is attained at higher blowing ratio. But for LA203A airfoil investigation was done only at two blowing ratios (0.1and 0.2). It was found that within this range of blowing ratios, performance of high lift airfoil LA203A increases (both in terms of attaining maximum lift coefficient and gain in stalling angle of attack) with the increase of blowing ratio.

Page 1-33 © MAT Journals 2018. All Rights Reserved

The study of blowing on thick airfoil shows that, with the increase in moment coefficient, lift increases and drag decreases as a result overall aerodynamic performance increases. It also reveals that increase in blowing ratio increases the lift. This study also predicts that at lower angles of attack (i.e., at 10 degrees and 16 degrees) mid chord slots have better control in increasing lift compared to leading edge slot whereas the opposite is true at higher angles of attack (at 22 degrees and 29 degrees).

The study of blowing on thick elliptical airfoil shows that lift increases with the increase in moment coefficient and it is equally true for three different blowing jet widths and four different Reynolds number. It also proves that lift increases with the increase in blowing ratio but this more effective on wider jet widths compared to that of narrower jet widths. To have a wider vision on the effect of jet width on the performance of thick elliptical airfoil it represents a graph of lift coefficient versus moment coefficient for six different blowing jet width which establishes the fact that there is an optimum blowing jet width beyond which aerodynamic performance (in terms of lift coefficient) drops.

This study also investigated the effect of blowing angle on the aerodynamic performance of thick elliptical airfoil (both in terms of lift and drag coefficient) for two different jet widths and two different Reynolds number and showed that better performance is attained for 90 degree blowing angle. Another graph which shows the effect of blowing angles (four angles 30, 45, 60, 90 were considered) on the lift curve, proves that better performance is achieved at lower blowing angles compared to the higher blowing angles.

Study of blowing on NACA 0012 and Aerospatiale A airfoil shows that lift coefficient increases with the increase in blowing ratio which is true for both the airfoils at three different jet diameters to chord ratios. For Aerospatiale A airfoil, drop in drag is achieved only when the jet diameter increases. NACA 0012 airfoil follow the same conclusion with an exception at blowing ratio 2.

This also concludes that for turbo machinery (compressor and turbine cascade) having higher blowing ratio (2) is a condition to get beneficial effect (in terms of pressure difference) from it.

Study of blowing on low Re airfoil flow reveals a different conclusion, that is, for low Re airfoil flows, as the blowing ratio increases the aerodynamic performance (in terms of lift coefficient, drag coefficient and lift to drag ratio) decreases. It is true for three different blowing angles (30, 45 and 90 degree) which are investigated in this study.

Future Direction

Even though enough researches have been conducted analytically, numerically and experimentally on flow control techniques and likely also on blowing but there are still scope for improvement in this field of research. There are several blowing parameters (like the number of blowing slots, slots entrance or exit angle, slot arrangements, oscillatory blowing etc.) the effect of who's on control performance can be investigated in an organized and systematic manner which may make this field of research richer and can be more beneficial when the results will be applied on real life applications. Thus, future researches can focus on these areas.

REFERENCES

1. Korayem M H, Zehfroosh A, Tourajizadeh H and Manteghi S, Optimal motion planning of non-linear

Page 1-33 © MAT Journals 2018. All Rights Reserved

dynamic systems in the presence of obstacles and moving boundaries using SDRE: application on cable-suspended robot, 2014 *Nonlin. Dyn.* 76 1423-41
2. Korayem M H, Tourajizadeh H, Zehfroosh A and Korayem A H, Optimal path planning of a cable-suspended robot with moving boundary using optimal feedback linearization approach, 2014 *Nonlin. Dyn.* 78 1515-43
3. Korayem M H, Tourajizadeh H, Zehfroosh A and Korayem A H, Optimal regulation of a cable robot in presence of obstacle using optimal adaptive feedback linearization approach, 2015 *Robotica* 33 933-52
4. Bozorgnezhad A, Shams M, Kanani H, Hasheminasab M and Ahmadi G, Two-phase flow and droplet behavior in microchannels of PEM fuel cell, 2016 *Int. J. Hydr. Energ.* 4119164-81
5. Bozorgnezhad A, Shams M, Kanani H, Hasheminasab M and Ahmadi G, The experimental study of water management in the cathode channel of single-serpentine transparent proton exchange membrane fuel cell by direct visualization, 2015 *Int. J. Hydr Energ.* 402808-32
6. Bozorgnezhad A, Shams M, Kanani H and Hasheminasab M, Experimental Investigation on Dispersion of Water Droplets in the Single-Serpentine Channel of a PEM Fuel Cell, 2015 *J. Dispers. Sci. Tech.* 36 1190-7
7. D. C. Hazen, Boundary layer control, Journal of Fluid Mechanics, 29 (1968) 200-208
8. Joslin, R.D. and D.N. Miller, Fundamentals and applications of modern flow control2009: American Institute of Aeronautics and Astronautics
9. M. Gad-el-hak, Control flow: Passive, active and reactive flow management, Cambridge University Press, United Kingdom (2000) 25-35.
10. Shan H, Jiang L, Liu C. Direct numerical simulation of flow separation around NACA0012 airfoil. Computers and Fluids 2005;34(9):1096–114
11. Anders, S.G., W.L. Sellers, and A. Washburn, Active flow control activities at NASA Langley. AIAA paper, 2004. 2623(2)
12. Martinstetter M, Neihuis R, Franke M. Passive boundary layer control on a highly loaded low pressure turbine cascade. ASME Paper 2010; GT 2010-22739:1315–26.
13. Hecklau M, Wiederhold O, Zander V, King R, Nitsche W, Huppertz A, et al. Active separation control with pulsed jets in a critically loaded compressor cascade. AIAA Journal
14. Deng S, Jiang L, Liu C. DNS for flow separation control around an airfoil by pulsed jet. Computers and Fluids 2007;36(6):1040–60
15. Carnarius, A., et al. Numerical study of the optimization of separation control. 2007
16. Schetz, J.A., Foundations of Boundary layer theory for momentum, Heat, and Mass Transfer1984: Wiley Online Library.
17. Williams, J., "A Brief History of British Research on Boundary Layer Control for High Lift," Boundary Layer and Flow Control, Pergamon, New York, 1961, pp. 74–103.
18. Head, M. R., "History of Research on Boundary Layer Control for Low Drag in U.K.," Boundary Layer and Flow Control, Pergamon, New York, 1961, pp. 104–121
19. Flatt, J. "The History of Boundary Layer Control Research in the United States of America," Boundary Layer and Flow Control, Pergamon, New York, 1961, pp. 122–143
20. Lachmann, G.V., Boundary layer and flow control: its principles and application. Vol. 2. 1961: Pergamon.

Page 1-33 © MAT Journals 2018. All Rights Reserved

21. Gad-el-Hak, M., Flow control: passive, active, and reactive flow management2000: Cambridge Univ Pr.
22. M. B. Glauert, The application of the exact method of airfoil design, Aeronautical Research Council, R&M 2683 (1947)
23. J. H. Preston, N. Gregory and A. G. Rawcliffe, The theoretical estimation of power requirements for slot-suction airfoils with numerical results for two thick griffith type sections, Aeronautical Research Council, R&M 1577 (1948)
24. D. F. Abzalilov, L. A. Aksentev and N. B. IL'Inskii, The inverse boundary-value problem for an airfoil with a suction slot, Journal of Applied Mathematics and Mechanics, 61 (1) (1997) 75-82
25. Seifert, A., A. Darabi, and I.J. Wygnanski, Delay of airfoil stall by periodic excitation. Journal of aircraft, 1996. 33(4): p. 691-698
26. Tinapp, F. and W. Nitsche. On active control of high-lift flow. 1999.
27. Wu, J., A. Vakili, and J. Wu, Review of the physics of enhancing vortex lift by unsteady excitation. Progress in Aerospace Sciences, 1991. 28(2): p. 73-131.
28. Miranda, S., Active control of separated flow over a circular-arc airfoil, 2000, Citeseer.
29. R. E Dannenberg and J. A. Weiberg, Section characteristics of a 10.5 percent thick airfoil with area suction as affected by chordwise distribution of permeability, NACA Technical Note 2847 (1952)
30. D. M. Heugen, An experimental study of a symmetrical airfoil with a rear suction slot and a retractable flap, Journal of Royal Aeronautical Society, 57 (1953)
31. R. E. Dannenberg and J. A. Weiberg, Section characteristics of an NACA0006 airfoil with area suction near the leading edge, NACA Technical Note 3285 (1954).
32. H. J. Howe and B. J. Neumann, An experimental evaluation of a low propulsive power discrete suction concept applied to an axisymmetric vehicle, David W. Taylor Naval Ship R&D Center TM 16-82/02 (1982)
33. S. Dirlik, K. Kimmel, A. Sekelsky and J. Slomski, Experimental evaluation of a 50-percent thick airfoil with blowing and suction boundary layer control, AIAA Paper No. AIAA-92-4500 (1992)
34. Ekaterinaris, J.A., Prediction of active flow control performance on airfoils and wings. Aerospace science and technology, 2004. 8(5): p. 401-410.
35. Liu, Y., et al., Computational evaluation of the steady and pulsed jet effects on the performance of a circulation control wing section. AIAA paper, 2004. 56: p. 2004.
36. H. Schlichting, Boundary layer theory, McGraw-Hill, New York, USA (1968) 347-362
37. E. J. Richards and C. H. Burge, An airfoil designed to give laminar flow over the surface with boundary layer suction, Aeronautical Research Council, R&M 2263 (1943)
38. S. W. Walker and W. G. Raymer, Wind tunnel test on the 30 percent symmetrical griffth airfoil with ejection of air, Aeronautical Research Council, R&M 2475 (1946).
39. A. L. Braslow, A history of suction type laminar flow control with emphasis on flight research, NASA History Division, Monograph in Aerospace History, 13 (1999)
40. Y. Guowei, W. Shanwu, L. Ningyu and Z. Lixian, Control of unsteady vertical lift on an airfoil by leading-edge blowing suction, ACTA Mechanica Sinica (English Series), 13 (4) (1997) 304-312.
41. J. Z. Wu, X. Y. Lu, A. G. Denny, M. Fan and J. M. Wu, Post-stall flow

Page 1-33 © MAT Journals 2018. All Rights Reserved

control on an airfoil by local unsteady forcing, Journal of Fluid Mechanics, 371 (1998) 21-58
42. C. Nae, Synthetics jets influence on NACA0012 airfoil at high angle of attacks, AIAA Paper No. AIAA-98-4523 (1998)
43. S. S. Ravindran, Active control of flow separation over an airfoil, Report of Langley Research Center (1999).
44. D. P. Rizzetta, M. R. Visbal and M. J. Stank, Numerical investigation of synthetic jet flow fields, AIAA Journal, 37 (8) (1999) 919-927
45. L. Huang, P. G. Huang and R. P. LeBeau, Numerical study of blowing and suction control mechanism on NACA0012 airfoil, Journal of Aircraft, 41 (5) (2004) 1005-1013.
46. Zheng X, Zhang Y, Xing W, Zhang J. Separation control on axial compressor cascade by fluidic based excitation. J Turbomach 2011;133(4):041016.
47. Ludewig T, Mack M, Niehuis R, Franke M. Optimization of the blowing ratio for a low-pressure turbine cascade with active flow control; 2011. ETC2011 Paper No. 131.
48. C. R. Rosas, Numerical simulation of flow separation control by oscillatort fluid injection, Doctor of Philosophy Thesis, A&M University, Texas (2005)
49. N. K. Beliganur and P. Raymond, Application of evolutionary algorithms to flow control optimization, Report of University of Kentuchky (2007)
50. Wong, C. and K. Kontis, Flow control by spanwise blowing on a NACA 0012. Journal of aircraft, 2007. 44(1): p. 337-340
51. Schatz, M. and F. Thiele, Numerical study of high-lift flow with separation control by periodic excitation. AIAA paper, 2001. 296: p. 2001.
52. Svorcan J M, Fotev V G, Petrović N B and Stupar S N, Two-dimensional numerical analysis of active flow control by steady blowing along foil suction side by different URANS turbulence models, thermal science, Year 2017, Vol. 21, Suppl. 3, pp. S649-S662
53. Moshfeghi M, Shams S and Hur N, Aerodynamic performance enhancement analysis of horizontal axis wind turbines using a passive flow control method via split blade, 2017 *J. Wind Eng. Ind. Aerodyn.* 167 148-59
54. Lee S, Loth E, Babinsky H. Normal shock boundary layer control with various vortex generator geometries. Computers and Fluids 2011;49(1):233–46.
55. Bai T, Liu J, Zhang W, Zou Z. Effect of surface roughness on the aerodynamic performance of turbine blade cascade. Propulsive Power Res 2014;3(2):82–9.
56. Bruneau CH, Creuse EC, Depeyras D, Gillieron P, Mortazavi I. Coupling active and passive technique to control the flow past square back Ahmed body. Computers and Fluids 2010;39(10):1875–92.
57. D. You and P. Moin, Active control of flow separation over an airfoil using synthetic jets, Journal of Fluids and Structures, 24 (8) (2008) 1349-1357.
58. S. H. Kim and C. Kim, Separation control on NACA23012 using synthetic jet, Aerospace Science and Technology, 13 (4) (2009) 172-182.
59. M. S. Genc, U. Keynak and H. Yapici, Performance of transition model for predicting low re airfoil flows without/with single and simultaneous blowing and suction, European Journal of Mechanics B/Fluids, 30 (2) (2011) 218-235.
60. C. L. Rumsey and T. Nishino, Numerical study comparing RANS and LES approaches on a circulation control airfoil, International Journal of Heat and Fluid Flow, 32 (5) (2011) 847-864.
61. T. Lee and Y. Y Su, Unsteady airfoil with a harmonically deflected trailing

Page 1-33 © MAT Journals 2018. All Rights Reserved

edge flap, Journal of Fluids and Structures, 27 (8) (2011) 1411-1424.
62. E. Benini, R. Biollo and R. Ponza, Efficiency enhancement in transonic compressor rotor blades using synthetic jets: A numerical investigation, Applied Energy, 88 (3) (2011) 953-962.
63. B. Yagiz, O. Kandil and Y. V. Pehlivanoglu, Drag minimization using active and passive flow control techniques, Aerospace Science and Technology, 17 (1) (2012) 21-31.
64. K. Yousefi, S. R. Saleh and P. Zahedi, Numerical study of flow separation control by tangential and perpendicular blowing on the NACA 0012 airfoil, International Journal of Engineering, 7 (1) (2013) 10-24
65. K. Yousefi, S. R. Saleh and P. Zahedi, Numerical investigation of suction and length of suction jet on aerodynamic characteristics of the NACA 0012 airfoil, International Journal of Materials, Mechanics and Manufacturing, 1 (2) (2013) 136-142.
66. Launder BE, Spalding DE. The numerical computation of turbulent flows. Comput Meth Appl Mech Eng 1974;2(3):269–89.
67. Critzos CC, Heyson HH, Boswinkle RW Jr., Aerodynamic characteristics of NACA 0012 airfoil section at angle of attack from 0 deg to 180 deg; 1955. NACA TN3361.
68. Sandeep Eldho James, Abhilash Suryan, Jiss J Sebastian, Abhay Mohan, Heuy Dong Kim, Comparative study of boundary layer control around an ordinary airfoil and a high lift airfoil with secondary blowing, Computers & Fluids, Volume 164, 15 March 2018, Pages 50-63
69. Hanns F. Müller-Vahl, Christoph Strangfeld, Christian N. Nayeri, Christian O. Paschereit, and David Greenblatt. "Control of Thick Airfoil, Deep Dynamic Stall Using Steady Blowing", AIAA Journal, Vol. 53, No. 2 (2015), pp. 277-295.
70. Chunmei Chen, Roman Seele, and Israel Wygnanski. "Separation and Circulation Control on an Elliptical Airfoil by Steady Blowing", AIAA Journal, Vol. 50, No. 10 (2012), pp. 2235-2247.
71. Svorcan, J. M., Vasko G. Fotev, Nebojsa B. Petrovic, Slobodan N. Stupar, Two-Dimensional Numerical Analysis of Active Flow Control by steady blowing along airfoil suction siude by different URANS Turbulence models, THERMAL SCIENCE, Year 2017, Vol. 21, Suppl. 3, pp. S649-S662
72. M. Serdar Genç, Ünver Kaynak, Hüseyin Yapici, Performance of transition model for predicting low Re airfoil flows without/with single and simultaneous blowing and suction, European Journal of Mechanics - B/Fluids, Volume 30, Issue 2, March–April 2011, Pages 218-235

Page 1-33 © MAT Journals 2018. All Rights Reserved